NOAA OAR Special Report

PMEL Tsunami Forecast Series: Vol. 30

A Tsunami Forecast Model for Fajardo, Puerto Rico

Diego Arcas[1,2]

[1]Joint Institute for the Study of the Atmosphere and Ocean (JISAO), University of Washington, Seattle, WA

[2]NOAA/Pacific Marine Environmental Laboratory (PMEL), Seattle, WA

April 9, 2015

NOTICE from NOAA

Mention of a commercial company or product does not constitute an endorsement by NOAA/OAR. Use of information from this publication concerning proprietary products or the tests of such products for publicity or advertising purposes is not authorized. Any opinions, findings, and conclusions or recommendations expressed in this material are those of the authors and do not necessarily reflect the views of the National Oceanic and Atmospheric Administration.

Contribution No. 3369 from NOAA/Pacific Marine Environmental Laboratory
Contribution No. 2114 from Joint Institute for the Study of the Atmosphere and Ocean (JISAO)

Contents

List of Figures

List of Tables

Foreword

Tsunamis have been recognized as a potential hazard to United States coastal communities since the mid-twentieth century, when multiple destructive tsunamis caused damage to the states of Hawaii, Alaska, California, Oregon, and Washington. In response to these events, the United States, under the auspices of the National Oceanic and Atmospheric Administration (NOAA), established the Pacific and Alaska Tsunami Warning Centers, dedicated to protecting United States interests from the threat posed by tsunamis. NOAA also created a tsunami research program at the Pacific Marine Environmental Laboratory (PMEL) to develop improved warning products.

The scale of destruction and unprecedented loss of life following the December 2004 Sumatra tsunami served as the catalyst to refocus efforts in the United States on reducing tsunami vulnerability of coastal communities, and on 20 December 2006, the United States Congress passed the "Tsunami Warning and Education Act" under which education and warning activities were thereafter specified and mandated. A "tsunami forecasting capability based on models and measurements, including tsunami inundation models and maps..." is a central component for the protection of United States coastlines from the threat posed by tsunamis. The forecasting capability for each community described in the PMEL Tsunami Forecast Series is the result of collaboration between the National Oceanic and Atmospheric Administration office of Oceanic and Atmospheric Research, National Weather Service, National Ocean Service, National Environmental Satellite, Data, and Information Service, the University of Washington's Joint Institute for the Study of the Atmosphere and Ocean, National Science Foundation, and United States Geological Survey.

NOAA Center for Tsunami Research

Abstract

The island of Puerto Rico sits on a tectonic microplate, known as the Puerto Rico-Virgin Islands plate. This microplate separates the North American from the Caribbean plate. The trench separating the Puerto Rico-Virgin Islands plate, the Puerto Rico Trench, is the deepest region in the Atlantic Ocean. It extends for over 1700 km, running parallel to the northern coast of the island. The Muertos Trough, separating the Puerto Rico-Virgin Islands plate from the Caribbean plate, runs parallel to the southern coast of Puerto Rico. There is no quantitative information about large historical tsunami events for the island of Puerto Rico, so it is not possible to use such events to validate the forecast model for Fajardo, a town located on the island's northeastern coast. Accuracy of the results is therefore tested in this study by comparing the solution obtained with the forecast model and that obtained with a higher-resolution reference model for six synthetic mega-tsunami scenarios originating in different regions of the Caribbean Sea and Atlantic Ocean. In addition to these mega-tsunami scenarios, a more probable Mw 7.5 scenario is also simulated, as well as a micro-tsunami triggered by a seismic event in the South Sandwich Islands, located in the South Atlantic. Results from this study confirm that the Puerto Rico Trench poses the largest tsunami hazard to the town of Fajardo.

Chapter 1

Background and Objectives

The Pacific Marine Environmental Laboratory (PMEL) of the National Oceanic and Atmospheric Administration (NOAA) Center for Tsunami Research (NCTR) has developed a tsunami forecasting capability for operational use by NOAA's two Tsunami Warning Centers located in Hawaii and Alaska (Titov et al. 2005). The system is designed to efficiently provide basin-wide forecast of approaching tsunami waves, and of tsunami inundation for specific coastal locations. The system, termed Short-term Inundation Forecast of Tsunamis (SIFT), combines real-time tsunami event data with numerical models to produce estimates of tsunami wave arrival times and flooding at a coastal community of interest. The SIFT system integrates several key components: deep-ocean, real-time observations of tsunamis, a basin-wide pre-computed propagation database of water level and flow velocities based on potential seismic unit sources (Gica et al., 2008), an inversion algorithm to refine the tsunami source based on deep-ocean observations during an event (Percival et al., 2011), and optimized tsunami flooding forecast models. The objective of the present work is to construct a tsunami inundation model for Fajardo, Puerto Rico that can be used by the Tsunami Warning Centers to assess, in real time, the local impact of a tsunami generated anywhere in the Caribbean or the Atlantic Ocean.

The two most relevant bathymetric and tsunamigeneic features offshore of Fajardo are the Puerto Rico Trench and the Muertos Trough (see Figure 1). The Puerto Rico Trench is the result of the Caribbean and North American plates sliding past each other and is the deepest point in the Atlantic Ocean. The Muertos Trough is formed by the intersection of the Caribbean and the Puerto Rico-Virgin Islands microplate. Both have the potential for triggering large tsunami events, having generated large magnitude (Mw > 8.0) earthquakes in the past, such as the 1787 event, which is listed among the six most significant events in the last three centuries to impact the island of Puerto Rico (Table 1; Mann,2005). There are two additional areas in close proximity to the island that have generated earthquakes of smaller magnitude in the last couple of centuries. The events, although small, were large enough to trigger damaging tsunamis. One of these two areas is the Mona Canyon to the west of the island, source of the 1918 Mw 7.5 event listed in Table 1, which separates the island of Puerto Rico from La Hispaniola. The other is the Anegada Passage to the east, source of the 1867 Mw 7.5 event listed in Table 1, which separates Puerto Rico from the Virgin Islands. At a more local scale, the other relevant bathymetric feature offshore of Fajardo is the shallow stretch of water in the Anegada Passage connecting the island with the Virgin Islands. Tsunamis approaching from this direction may experience more energy dissipation than those approaching from the deeper waters to the north and south of the island. This report details the development of a high-resolution tsunami forecast model for

Fajardo, Puerto Rico, including development of the bathymetric grids, model validation, and stability testing with a set of synthetic mega-tsunami (Mw 9.3) events. Inundation results from such artificial events are presented in later sections.

Chapter 2

Forecast Methodology

A high-resolution inundation model was used as the basis for the operational forecast model to provide an estimate of wave arrival time, height, and inundation immediately following tsunami generation. Tsunami forecast models are run in real time while the tsunami in question is propagating across the open ocean. These models are designed and tested to perform under very stringent time constraints given that time is generally the single limiting factor in saving lives and property. The goal is to maximize the amount of time that an at-risk community has to react to a tsunami threat by providing accurate information quickly. To this end, the tsunami propagation solution in deep water is pre-computed in the linear wave regime and used to force the inundation forecast models during the last stage of tsunami propagation and runup.

The tsunami forecast model, based on the Method of Splitting Tsunami (MOST), emerges as the solution in the SIFT system by modeling real-time tsunamis in minutes. SIFT employs high-resolution bathymetric grids constructed by the National Geophysical Data Center (NGDC) or, in limited instances, internally. Each forecast model consists of three nested grids with increasing spatial and temporal resolution for simulation of wave inundation onto dry land. The forecast model utilizes the most recent bathymetry and topography available to reproduce the correct wave dynamics during the inundation computation. Forecast models are constructed for at-risk populous coastal communities in the Pacific and Atlantic oceans. Previous and present development of forecast models in the Pacific (Titov et al., 2005; Titov, 2009; Tang et al., 2009; Wei et al., 2008) have validated the accuracy and efficiency of the forecast models currently implemented in the SIFT system for real-time tsunami forecast. The model system is also a valuable tool in hindcast research. Tang et al. (2009) provides forecast methodology details.

Chapter 3

Model Development

Modeling of coastal communities is accomplished by the development of a set of three nested grids that telescope down from a large spatial extent to a grid that finely defines the bathymetric and topographic features of the community under study. For Fajardo, Puerto Rico, the original bathymetric and topographic grid data used to develop the forecast model were provided by the NGDC. Details of data gathering and grid construction techniques used by the NGDC in the generation of the original grid are provided by Taylor et al. (2007). For each community, data are compiled from a variety of sources to produce a digital elevation model referenced to Mean High Water in the vertical and to the World Geodetic System 1984 in the horizontal (http://ngdc.noaa.gov/mgg/inundation/tsunami/inundation.html). From these digital elevation models, a set of three high-resolution reference grids are constructed, which are then "optimized" to run in an operationally specified period of time.

As new digital elevation models become available, forecast models will be updated and report updates will be posted at *http://nctr. pmel.noaa.gov/forecast_reports*.

The final forecast model grids for Fajardo are based on the original set of grids developed by Aurelio Mercado from the University of Puerto Rico. Whenever available, topographic data have been added to the outer and intermediate grids. In addition, some instabilities that appeared in the original reference grids when tested with the standard tsunami scenarios for the Atlantic have been fixed, and some artifacts and singularities (such as single node sinks) that were probably present in the original set of grids provided by NGDC have been corrected.

3.1 Forecast area

Figure 2 shows an aerial view of the town of Fajardo with the Playa Sardinera marina in the center of the image. The study area for this forecast model is centered in the City of Fajardo. Fajardo is located on the northeastern coast of the island of Puerto Rico, facing the Atlantic Ocean. The inundation grid (innermost grid) has been designed to include the entire city of Fajardo, its airport and the nearby community of Ceiba, located approximately 9.6 km to the south. The location of Jose Aponte de la Torre International Airport to the south of Ceiba has also been included in the inundation grid.

Fajardo has a population of 36,971 (US Census, 2010) and it is the main recreational boating hub in Puerto Rico with the largest recreational marina in the Caribbean, Puerto del Rey. It is also the departure port to the Puerto Rican islands of Culebra and Vieques, as well as the British

Virgin Islands. (http://en.wikipedia.org/wiki/Fajardo_Puerto_Rico)

The northeastern coast of the island of Puerto Rico is protected from tsunamis by an offshore shallow water area bounded by the island of Culebra to the north, Vieques to the south and the Virgin Islands to the east. The islands of Culebra and Vieques have been included in the intermediate grid of the forecast model, while the Virgin Islands have been included in the outermost grid.

3.2 Historical events and data

A NOS-operated tide gauge (9753216) was deployed on the Fajardo pier on 17 February 1964 and moved to its current location (18.33523147° N, 65.6308797° W) on 11 March 2007. The tide gauge is located in the commercial harbor to the south end of the city's waterfront, close to the Fajardo-Vieques ferry line pier. The lower right panel of Figure 3 shows the location of the tide gauge within the inundation (innermost) grid of the forecast model. However, no tide gauge data of recent tsunamis at this location were found, so no such data could be used in the historical validation of this forecast model. Consequently, the validation of the forecast model was based on the comparison of high-resolution reference model results with forecast model results.

3.3 Model setup

Setup of the computational grids for the MOST code (Titov and Synolakis, 1998) requires a total of three nested grids, for which the outermost grid, A, has the lowest spatial resolution but covers the largest area, and the innermost grid, C, has the highest spatial resolution but covers a reduced geographical area. The code makes use of an additional intermediate grid, B, with medium resolution and spatial coverage. Each interior grid area is completely enclosed in the area covered by the immediate exterior grid, and inundation is computed only in the innermost grid (C Grid). The purpose of the set of three nested grids is to ensure that, as the tsunami wavelength shrinks when it travels from deep to shallow waters, the model maintains an approximately constant number of grid nodes per wavelength.

This set of three nested grids is forced by a pre-computed solution on an ocean-wide grid at lower resolution (4 arc min × 4 arc min). The resolution of the propagation grid was selected to adjust numerical dispersion in the code, to mimic the effect of physical dispersion (Burwell et al., 2007).

During the development of an operational forecast model, a higher-resolution set of grids, referred to as the reference model, is generated first. The purpose of the reference model is to evaluate grid convergence between a high-resolution model and the forecast model, ensuring that the solution obtained with the lower-resolution forecast model is consistent with that computed with the high-resolution reference model.

Several factors are taken into account in the design of the Fajardo model grids. One is the presence of extensive areas of extremely shallow water around the Caribbean arc. Tsunami waves propagating over these shallow water regions will experience a shortening of their wavelength as they approach the island of Puerto Rico. It is important, therefore, to model wave propagation over these areas using a higher-resolution grid than that used for the simulations stored in the deep-water propagation database (4-arc-min resolution). This is accomplished in the

present model by extending the outermost grid of the set of three nested grids (A Grid) toward the east and south of Puerto Rico. The resolution of the A Grid in the present model is 47.24 arc sec in the zonal direction and 4 arc sec in the meridional direction, permitting the resolution of much higher frequency waves over shallow regions than the 4-arc-min propagation database grid.

In addition, the A grid used in the current forecast model is identical to the A grid used in other Caribbean region forecast models, such as that for the Charlotte Amalie model in the U.S. Virgin Islands. This setup may be advantageous in future configurations of SIFT software, since it will make it possible to compute the A grid only once and share the computation results with all forecast models located within the geographical extent of the grid, avoiding multiple computations of the same grid for different forecast models. Figures 4 and 5 show grid coverage area and relative grid position with respect to the community and local bathymetric features for the reference and forecast models, respectively. Table 2 summarizes the parameters and model setup for each set of grids.

Chapter 4

Results and Discussion

Typically, three types of tests are performed to assess the forecast model convergence, accuracy, and robustness characteristics. However, in the case of Fajardo, Puerto Rico, since no historical data are available, accuracy tests based on historical events could not be performed.

To assess model convergence, results obtained with the reference model were compared with those obtained with the forecast model to confirm consistency of results, at least for the leading tsunami waves. This type of test is not, strictly speaking, a grid convergence test in the sense used in computational science, since the solution is compared on grids with varying resolution, coverage, and bathymetric information; it does, however, provide a good estimate of the similarities and discrepancies between the solution of a more accurate, high-resolution model of the area and that of a coarser-resolution accelerated forecast model.

Robustness tests include the simulation of six mega-tsunami events generated by Mw 9.3 earthquakes, one medium magnitude (Mw 7.5) event, and one small magnitude (micro-tsunami, Mw 6.2) event throughout the Caribbean and Atlantic basin. Figure 6 shows the epicenter locations of these artificial events. Details of these synthetic scenarios are provided in Table 3. Forecast model simulations proved to be free of instabilities during 24 hr of simulation for each of these synthetic events.

Studying the results obtained during the development of the forecast model for Fajardo, it can be observed that tsunamis arriving from the northern part of the island tend to generate the largest wave amplitudes in the town of Fajardo and around its coastal areas. It is also particularly evident in the maximum elevation plots of Figures 7 and 8 (synthetic scenarios 1 and 2, Table 3) that an island chain on the northeastern corner of the island, extending offshore to the east, seems to behave as a natural barrier for tsunamis originating north of the island, therefore mitigating their impact on Fajardo. This island chain seems to be mostly uninhabited. However, the mitigating effect of the island chain is clearly not enough to protect the town of Fajardo from tsunamis arriving from the north, since synthetic scenario 2 (Table 3; Figure 8) still represents the worst case scenario in this study.

4.1 Model validation

As there are no recorded historical tsunami events for Fajardo, the validity of the forecast model was assessed by comparing the forecast model solution with that obtained using the high-resolution reference model for the eight synthetic scenarios discussed above. Since most of

the tested scenarios are simulated Mw 9.3 events, this set of tests was also used to establish the stability of the forecast model.

4.2 Model stability testing using synthetic scenarios

During model stability testing, eight synthetic tsunamis (generated by Mw 9.3, Mw 7.5, and Mw 6.2 earthquakes) were simulated using the forecast model (Table 3). Each of the six extreme synthetic mega-tsunami events is constructed along a 1000 km long × 100 km wide fault plane with uniform slip amount of 25 m along the fault. The output from the code at every time step was visualized and inspected for instabilities. The cause of any instability was corrected and a final set of forecast grids emerged from the process. Most of the forecast model instabilities were associated with deficient resolution to distinguish small bathymetric and topographic features.

Six of the eight synthetic events used as test cases in this study were generated by earthquakes with epicenters located at different points along the Caribbean arc. The micro-tsunami (Mw 6.2) event was designed to be generated by a far-field earthquake in the South Sandwich Islands. Time series comparison of the results obtained with the high-resolution reference model and with the forecast model show very good agreement, with almost a one-to-one comparison between the two signals up to 12 hr into the event, as evidenced in Figures 7 to 14. However, some of the differences between the reference and forecast model simulations in the later waves appear as slight discrepancies in the maximum amplitude of the wave train between both simulations, such as is the case for synthetic scenarios 1 and 5 (Table 3; Figures 7 and 11, respectively). Nevertheless, most of the simulations show excellent agreement between the two models, even 12 hr into the simulation.

Of all six mega-tsunami events tested, synthetic scenario 2, an event originating from Atlantic source zone ATSZ 48–57, poses the largest tsunami hazard to Fajardo, with predicted wave amplitude of approximately 5 m at the Fajardo tide gauge (Figure 8). Not surprisingly, synthetic scenario 2 represents a Mw 9.3 tsunami scenario generated in the Puerto Rico Trench, directly offshore and to the north of the island of Puerto Rico. This is the worst case scenario for Fajardo of all cases tested during the present study as evidenced in Figures 7 to 14 and in Appendix D Figures D1 and D2. It is important to note here that synthetic scenario 2 is also the worst case scenario for the town of Arecibo, located on the northern coast of Puerto Rico; however, the computed wave amplitude at Arecibo for such an event is almost 3 times larger than that computed in Fajardo. The two main reasons for the reduced wave heights at Fajardo are (1) the presence of an island chain along the northeastern corner of the island that provides a good amount of protection from tsunamis generated in the Puerto Rico Trench, as noted earlier in this chapter, and (2) the fact that tsunami waves from the Puerto Rico Trench must diffract around the island to reach the town of Fajardo, whereas Arecibo is directly exposed to tsunamis originating in the Trench.

Synthetic scenario 2 is also the worst case scenario for the eastern seaboard of the United States. However, this scenario was designed merely to test the stability and performance of the forecast model during a very large local event. The credibility of such a scenario as a viable earthquake event at that location is not being considered in this study. Consequently, these results should not be interpreted as a tsunami hazard study for Fajardo or the eastern seaboard of the U.S., but rather as numerical exercises to test the computational stability of the forecast model.

Additional cases from Table 3 generating a significant amount of inundation at Fajardo are synthetic scenarios 1, 3 and 5, with tsunamis originating along the eastern segment of the Caribbean arc, along the coast of Hispaniola, and off of the Caribbean coastline of Honduras, respectively. Figures 7 to 14 show the comparison between the inundation extents and maximum wave amplitudes for all eight synthetic scenarios computed with the reference and forecast models.

Chapter 5

Summary and Conclusions

A set of tsunami forecast grids has been developed for operational use by the Tsunami Warning Centers in conjunction with the Method of Splitting Tsunami code. Two sets of grids were developed: a high-resolution set intended to provide reference values, and a forecast set designed to minimize processor run time and to provide real-time tsunami estimates in Fajardo, Puerto Rico.

During model development, some geographical features unique to Fajardo, such as the presence of an island chain off the northeastern coast of the island of Puerto Rico, were observed to play a significant role in attenuating the impact of a tsunami generated along the Puerto Rico Trench, as reflected in the reduced wave heights computed at the Fajardo tide gauge when compared with those calculated at other locations along the north coast of the island, such as Arecibo, for the same event. Despite the mitigating effect of these islands, such an event seems to generate the largest tsunami wave amplitude in and around Fajardo.

The standard procedure of testing the accuracy of the model with data from historical events and evaluating computed results with observations, followed in the development of other forecast models in the Pacific Ocean, could not be performed in this case due to the lack of good quantitative data for recent historical tsunami events in the area. Therefore, accuracy of the forecast model had to be evaluated in conjunction with its stability by comparing the forecast results of a series of synthetic mega-tsunami events with results obtained using a set of higher-resolution grids.

Even though the magnitude of synthetic events selected to perform stability tests on the forecast model may not necessarily represent credible seismic scenarios, the directivity of their tsunamis can be interpreted as an indicator of what regions of the Caribbean pose the largest tsunami hazard for Fajardo. In this respect, the results of our simulations show that an event in the Puerto Rico Trench immediately offshore and north of the island of Puerto Rico (synthetic scenario 2, Table 3) represents the worst case scenario, followed by an event from the eastern boundary of the Caribbean arc (synthetic scenario 1, Table 3). However, the town of Fajardo seems to be more protected from tsunamis than other locations on the island, mainly because tsunamis can only have a direct impact on Fajardo if they are generated to the east of Puerto Rico. In this case, tsunami waves will have to propagate over the shallow areas of Anegada Passsage and around the Virgin Islands before making landfall in Fajardo. Propagation over these shallow regions will probably dissipate a substantial amount of energy by generating high-frequency waves; consequently, the tsunami waves arriving at Fajardo may be somewhat weakened.

The decision to include the shallow water areas along the Caribbean arc in the design of the forecast model grids by using the highest grid resolution possible and to share the A grid with the forecast model for Charlotte Amalie, U.S. Virgin Islands, was determined to have minor impact on processor run time. The forecast model was still capable of simulating 4 hr of tsunami activity in 12.2 min of wall-clock time on an Intel Xeon E5670 2.3 processor.

Chapter 6

Acknowledgments

The authors wish to thank the NOAA Center for Tsunami Research group for discussions, comments, and editorial assistance, and Sandra Bigley for technical assistance and editorial review of this report. Collaborative contributions of the National Weather Service, the National Geophysical Data Center, and the National Data Buoy Center were invaluable. This research is funded by the NOAA Center for Tsunami Research (NCTR). The authors would like to thank the modeling group of NCTR for their helpful suggestions and discussions. This publication was partially funded by the Joint Institute of the Atmosphere and Ocean (JISAO) under NOAA Cooperative Agreement Numbers NA10OAR4320148 and NA08OAR4320899. This is JISAO contribution number 2114 and PMEL contribution number 3369.

Chapter 7

References

Burwell, D., E. Tolkova, H. A. Chawala, J. (2007). Diffusion and dispersion characterization of a numerical tsunami model. *Ocean Modelling*, Vol. 19, Issues 1-2, ISSN 1463-5003.52

Gica, E., M. Spillane, V.V. Titov, C. Chamberlin, J.C. Newman (2008). Development of the forecast propagation database for NOAA's Short-term Inundation Forecast for Tsunamis (SIFT). *NOAA Tech. Memo*. OAR PMEL-139, 89 pp.

Mann, Paul (Editor), (2005). Active Tectonics and Seismic Hazards of Puerto Rico, the Virgin Islands, and Offshore Areas. The Geological Society of America, 2005. Special Paper 385.ISBN 0-8137-2385-x

Percival, D.B., D.W.. Denbo, M.C. Eble., E. Gica, H.O. Mofjeld, M.C. Spillane, L. Tang, V.V. Titov, (2011). Extraction of tsunami source coefficients via inversion of DART® buoy data. *Nat. Hazards*, 58(1), doi: 10.1007/s11069-010-9688-1, 587-590.

Tang, L., V.V. Titov, and C.D. Chamberlin (2009). Development, testing, and applications of site-specific tsunami inundation models for real-time forecasting. *J. Geophys. Res*, Vol.114, C12025, doi: 10.1029/2009JC005476, ISSN 1463-5003.52.

Taylor, L.A., B.W. Eakins, K.S. Carignan, R.R. Warnken, T. Sazonova and D.C. Schoolcraft. (2007). Digital Elevation Models for Puerto Rico: Procedures, Data Sources and Analysis. National Geophysical Data Center. June 22 2007.

Titov, V.V., and C.E. Synolakis (1998). Numerical modeling of tidal wave runup. *J. Waterw. Port Coast. Ocean Eng*, 124(4), 157-171.

Titov, V.V., F.I. González, E.N. Bernard, M.C. Eble, H.O. Mofjeld, J.C. Newman, and A.J. Venturato (2005). Real-time tsunami forecasting: Challenges and solutions. *Nat. Hazards.*, 35(1), 41-58.

Titov, V.V. (2009). Tsunami forecasting. In *The Sea*, Vol. 15, Chapter 12, Harvard University Press, Cambridge, MA and London, England, 371-400.

Wei, Y., E. Bernard, L. Tang, R. Weiss, V. Titov, C. Moore, M. Spillane, M. Hopkins, and U. KÏnoùglu. (2008). Real-time experimental forecast of the Peruvian tsunami of August 2007 for U.S. coastlines. *Geophys. Res. Lett.*, L04609, doi: 10.1029/2007GL032250.

U.S. Census.
http://factfinder2.census.gov/faces/tableservices/jsf/pages/productview.xhtml?pid=DEC_10_DP_DPDP1.

USGS Science for a Changing World, Earthquake and Tsunamis in PR and the U.S. VI

FIGURES

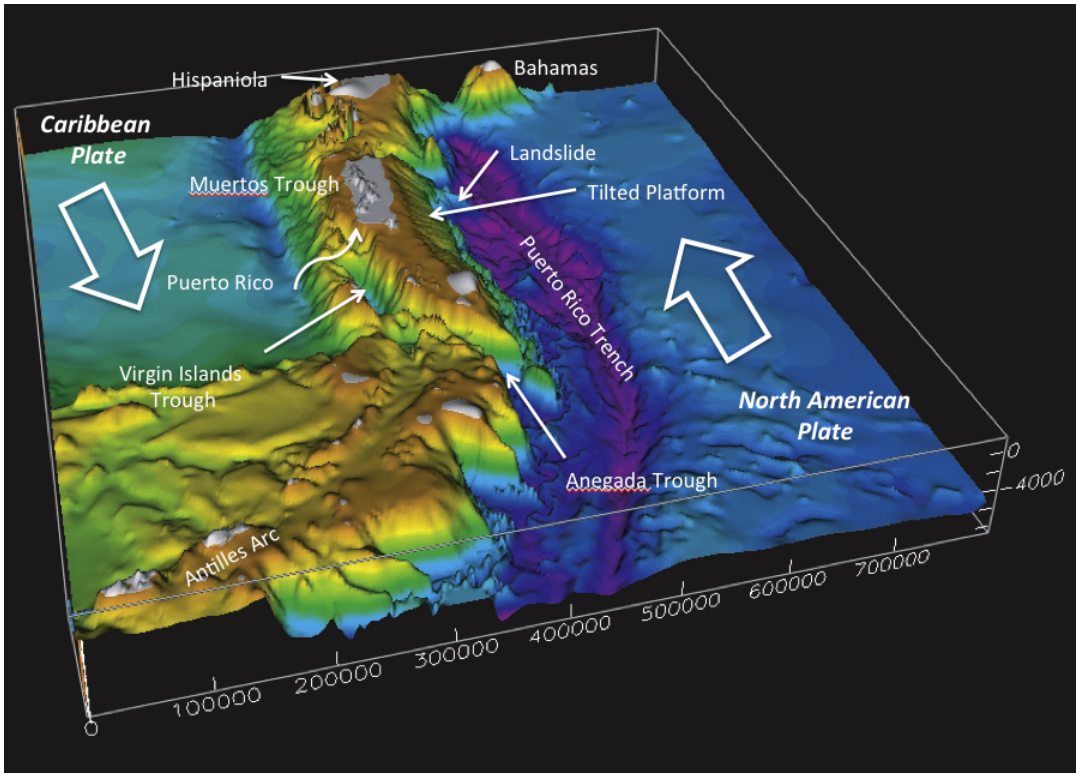

Figure 1: Schematic of tectonic motion and location of major bathymetric features in the neighborhood of Puerto Rico (from USGS Science for a Changing World, Earthquake and Tsunamis in Puerto Rico and the U.S. Virgin Islands).

Figure 2: Aerial view of Fajardo showing the largest of three recreational boating facilities in town (Google Maps).

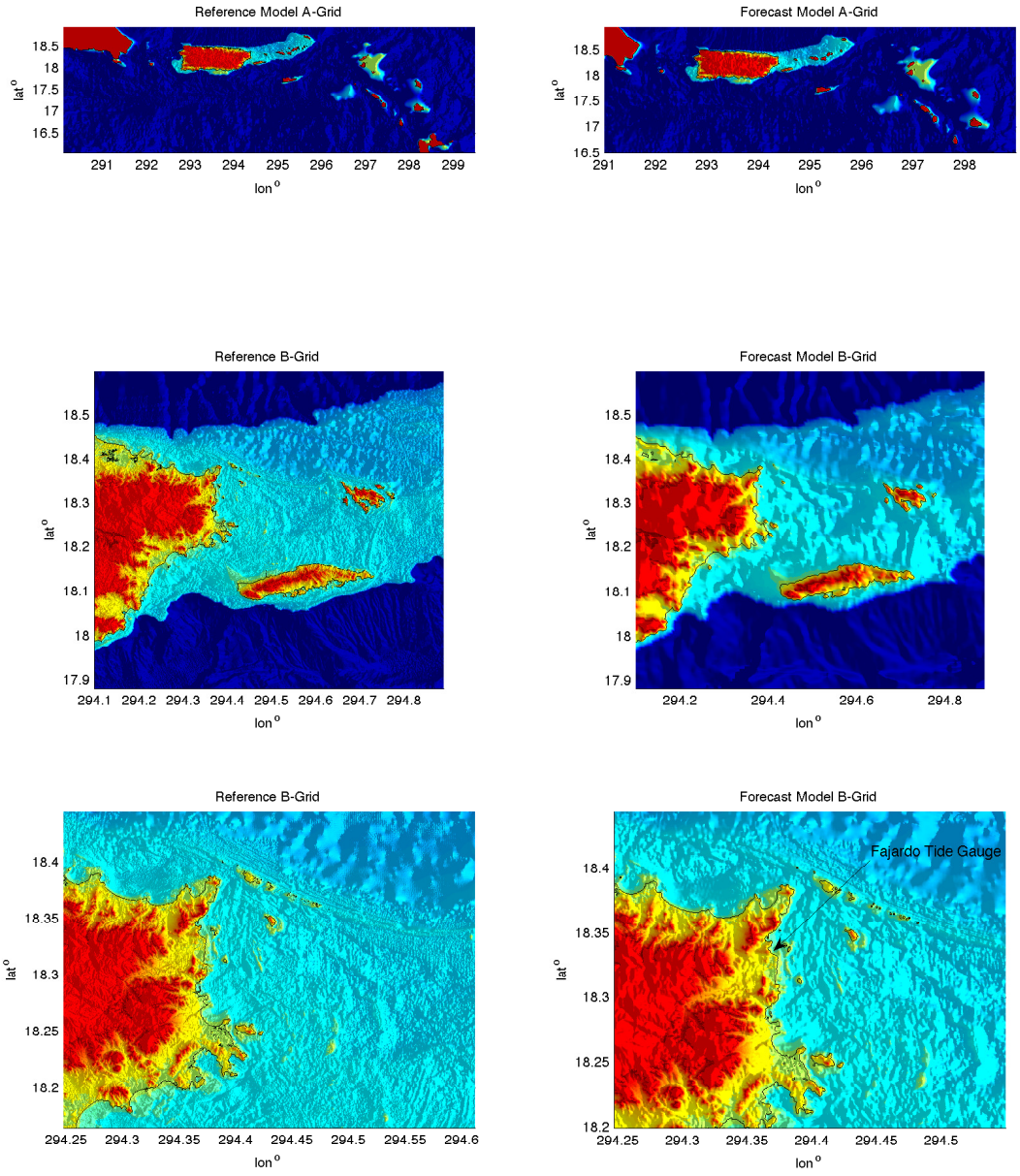

Figure 3: Comparison between the reference and forecast model grids. The location of the Fajardo tide gauge on the south side of the pier is indicated in the lower right panel.

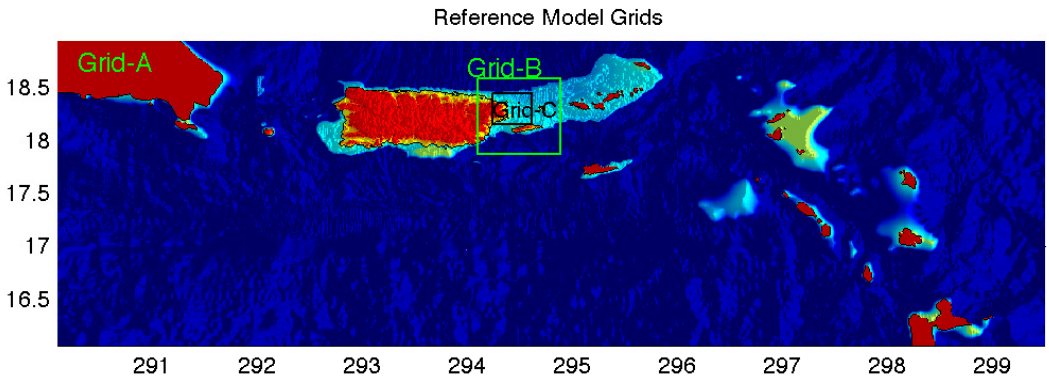

Figure 4: Map of the northeastern Caribbean arc showing the relative position of the reference model grids relative to Fajardo and the island of Puerto Rico.

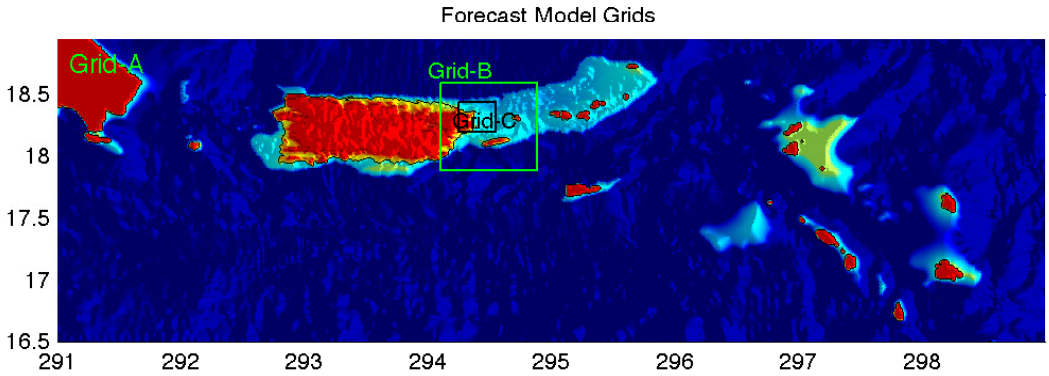

Figure 5: Map of the northeastern Caribbean arc showing the relative position of the forecast model grids relative to Fajardo and the island of Puerto Rico.

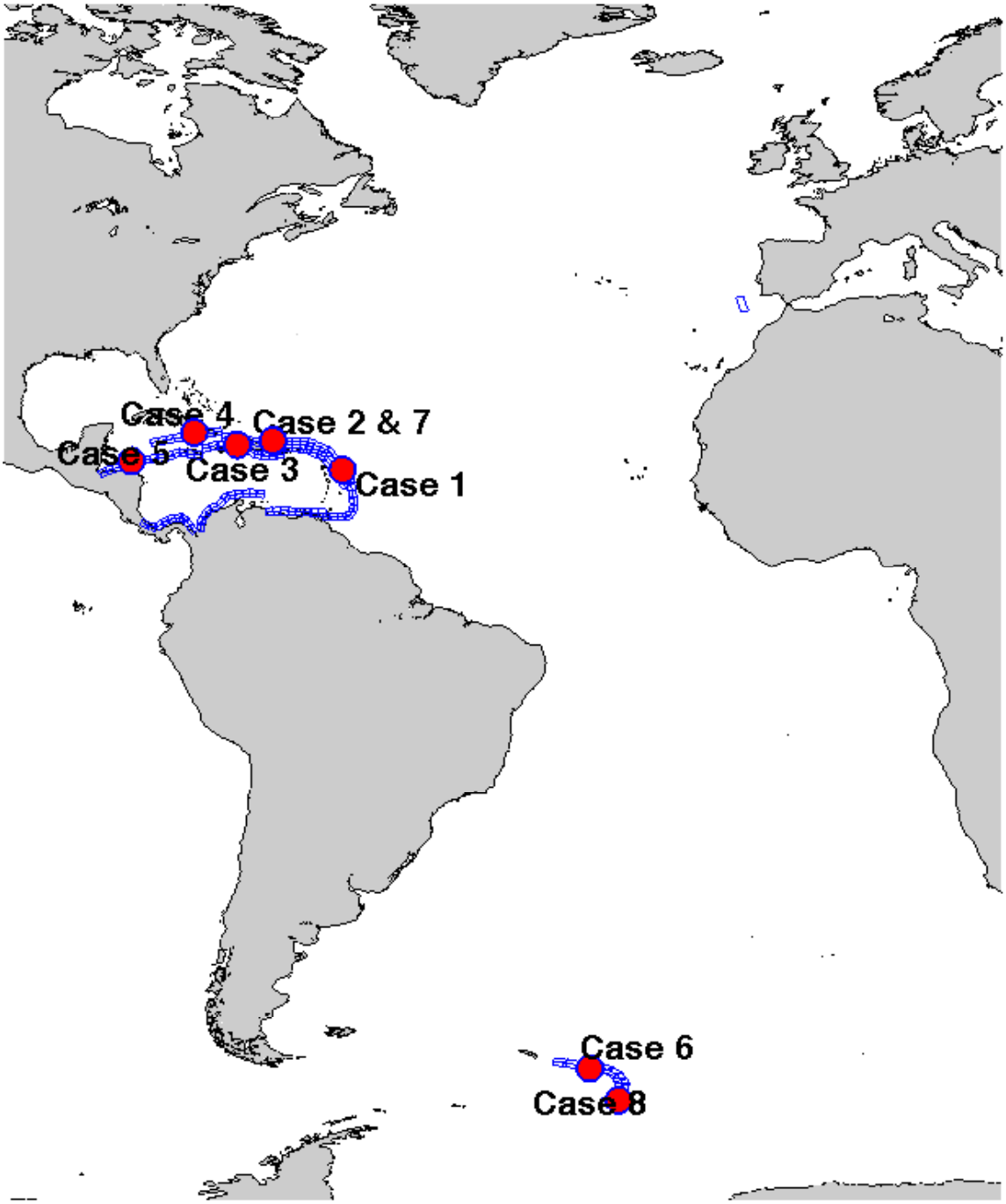

Figure 6: Location of the mid-rupture point of the 8 synthetic (Mw=9.3) events used in the model robustness tests, showing the relative position of Puerto Rico to the epicenter locations.

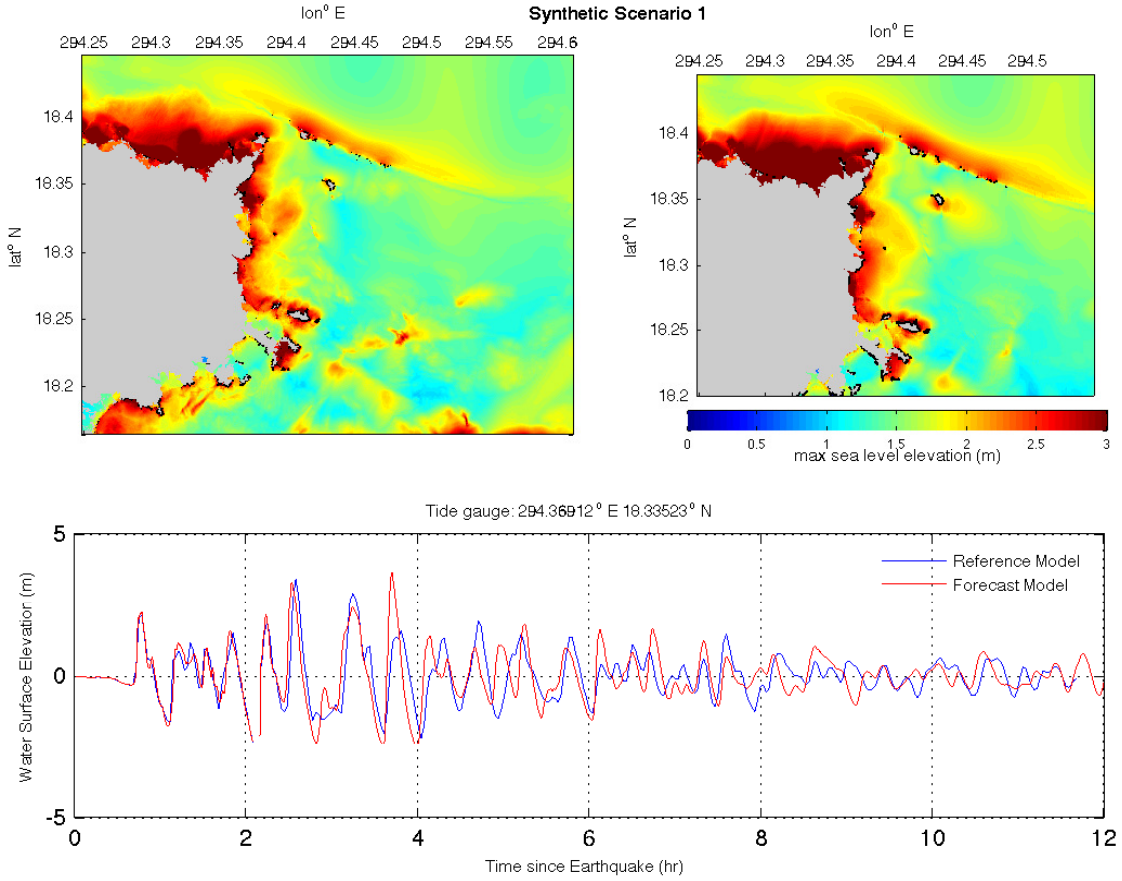

Figure 7: Maximum sea surface elevation computed with the reference (top left) and forecast (top right) models. Comparison at the Fajardo tide gauge of the forecast and reference models for Synthetic Scenario 1 (bottom).

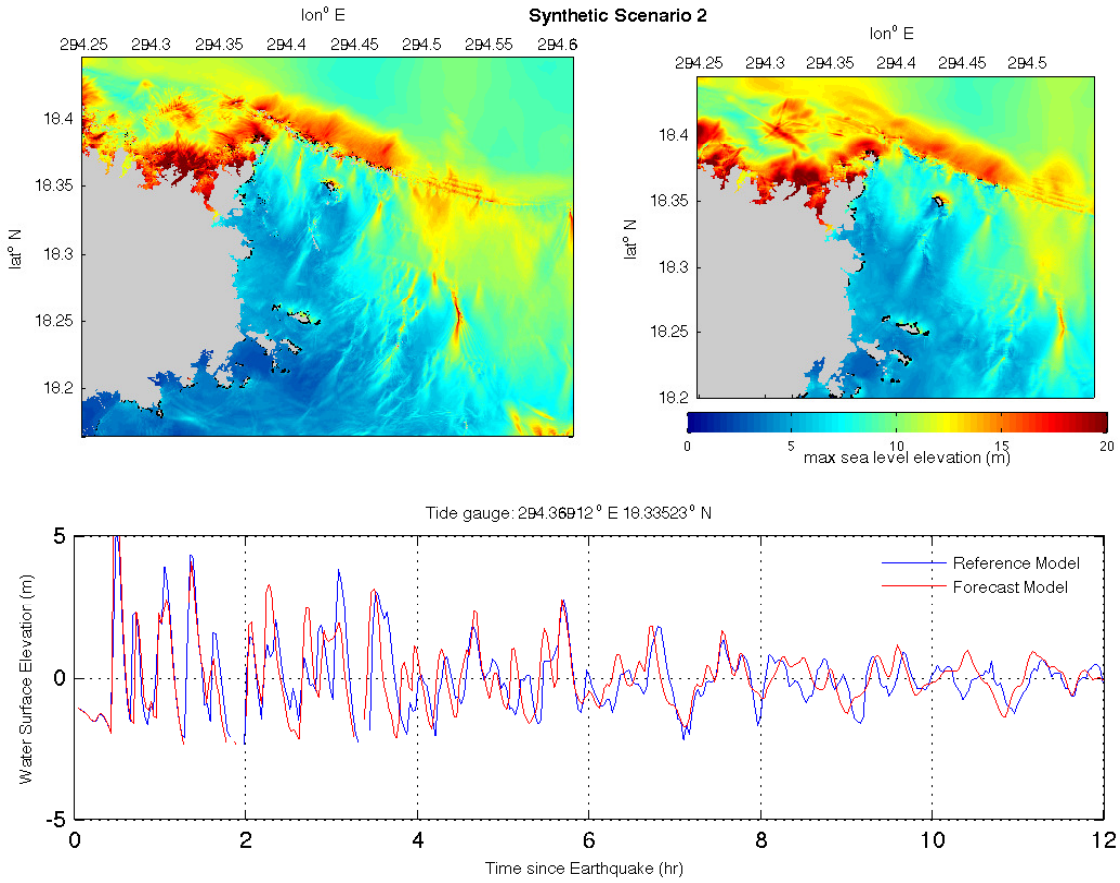

Figure 8: Maximum sea surface elevation computed with the reference (top left) and forecast (top right) models. Comparison at the Fajardo tide gauge of the forecast and reference models for Synthetic Scenario 2 (bottom).

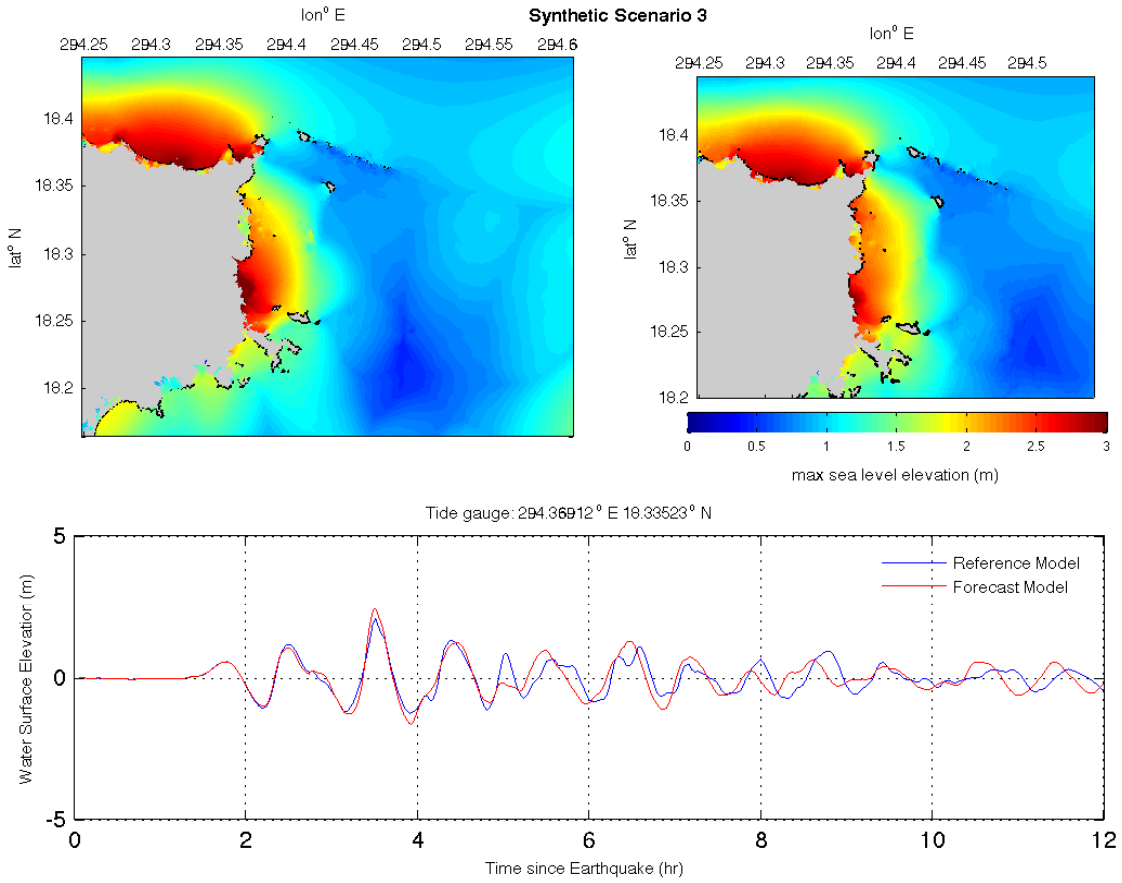

Figure 9: Maximum sea surface elevation computed with the reference (top left) and forecast (top right) models. Comparison at the Fajardo tide gauge of the forecast and reference models for Synthetic Scenario 3 (bottom).

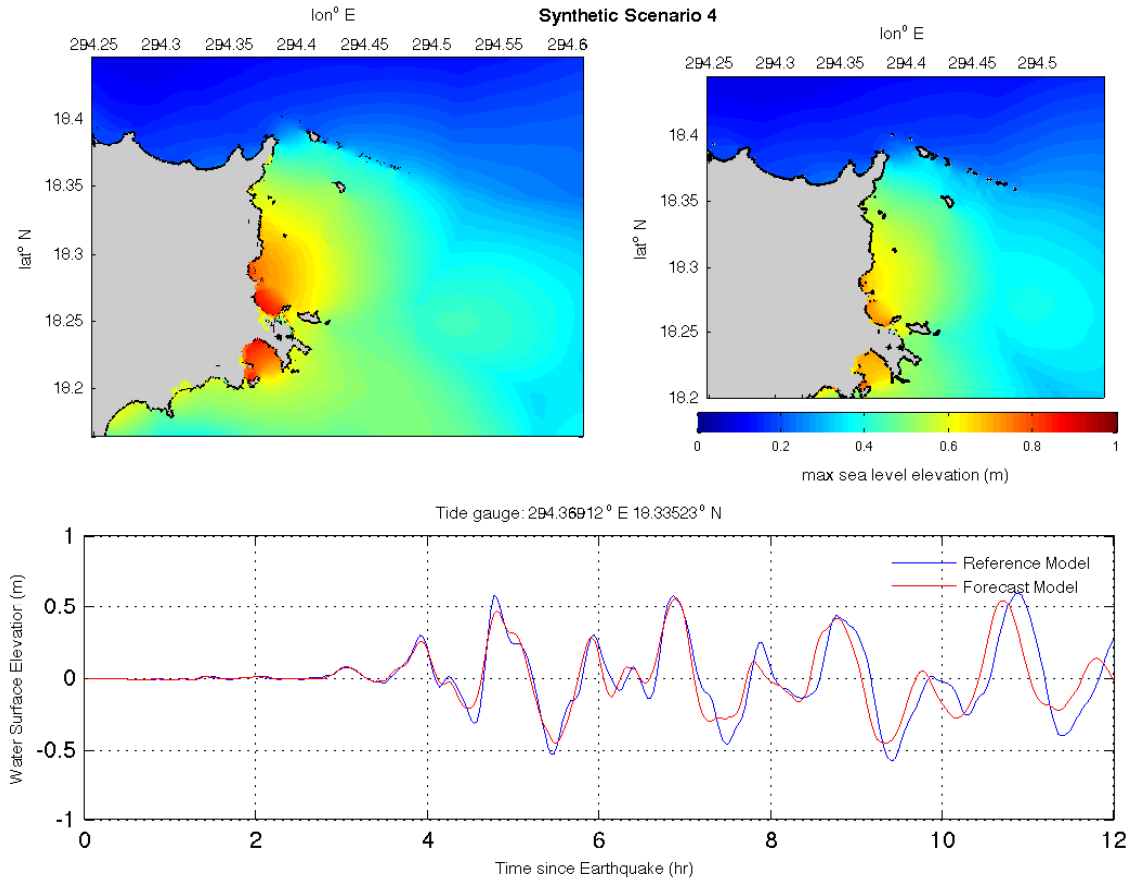

Figure 10: Maximum sea surface elevation computed with the reference (top left) and forecast (top right) models. Comparison at the Fajardo tide gauge of the forecast and reference models for Synthetic Scenario 4 (bottom).

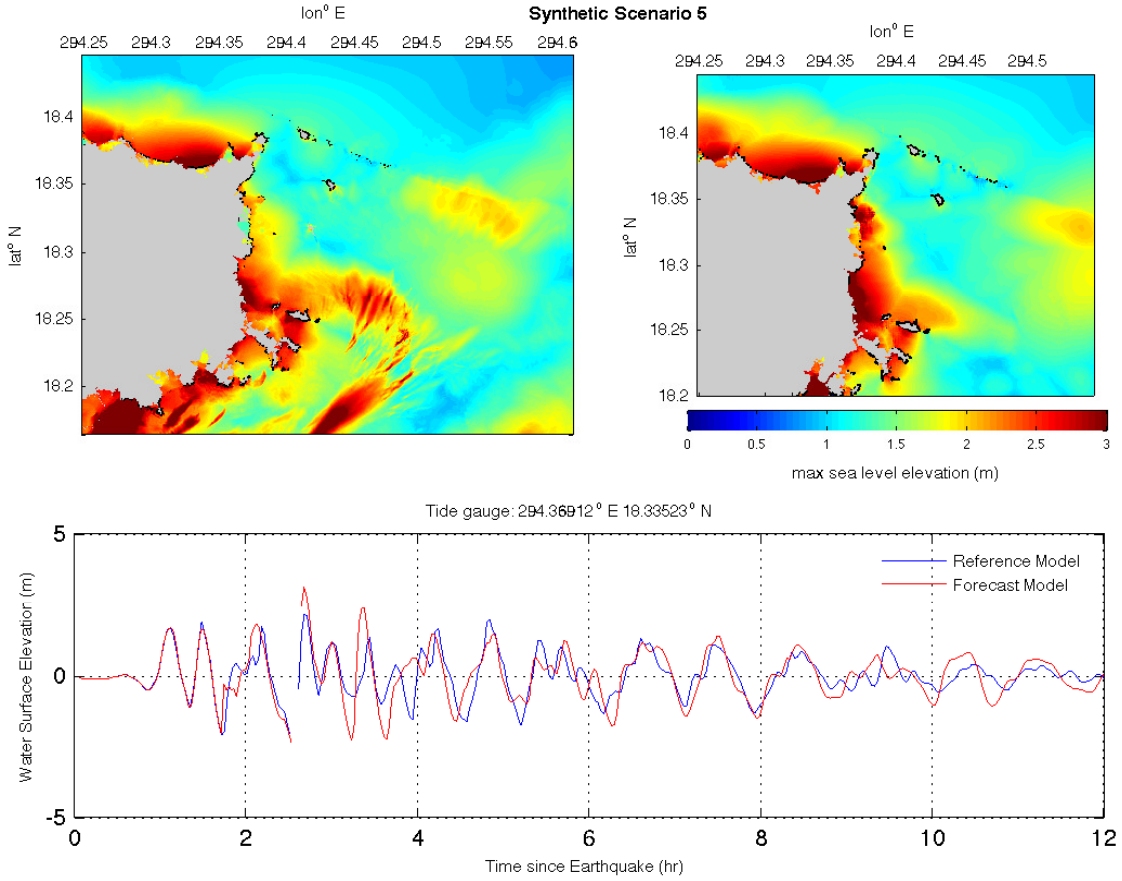

Figure 11: Maximum sea surface elevation computed with the reference (top left) and forecast (top right) models. Comparison at the Fajardo tide gauge of the forecast and reference models for Synthetic Scenario 5 (bottom).

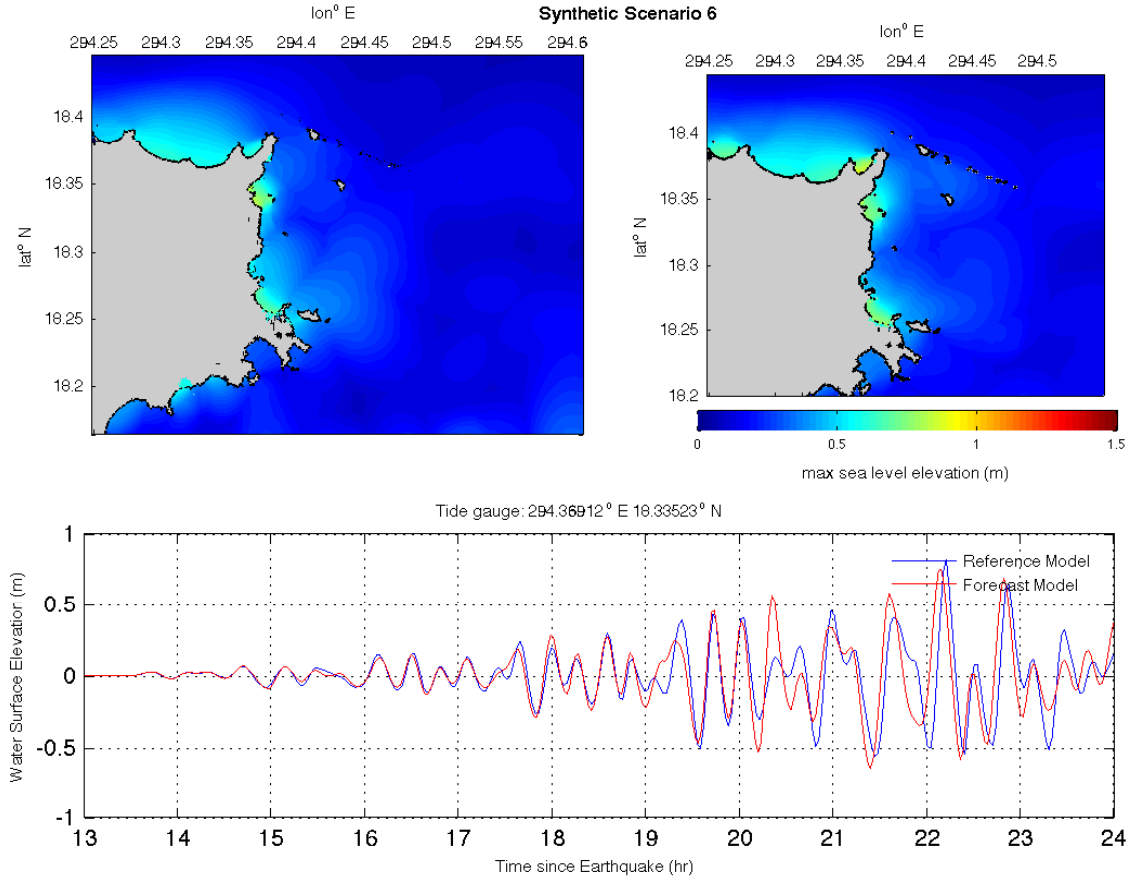

Figure 12: Maximum sea surface elevation computed with the reference (top left) and forecast (top right) models. Comparison at the Fajardo tide gauge of the forecast and reference models for Synthetic Scenario 6 (bottom).

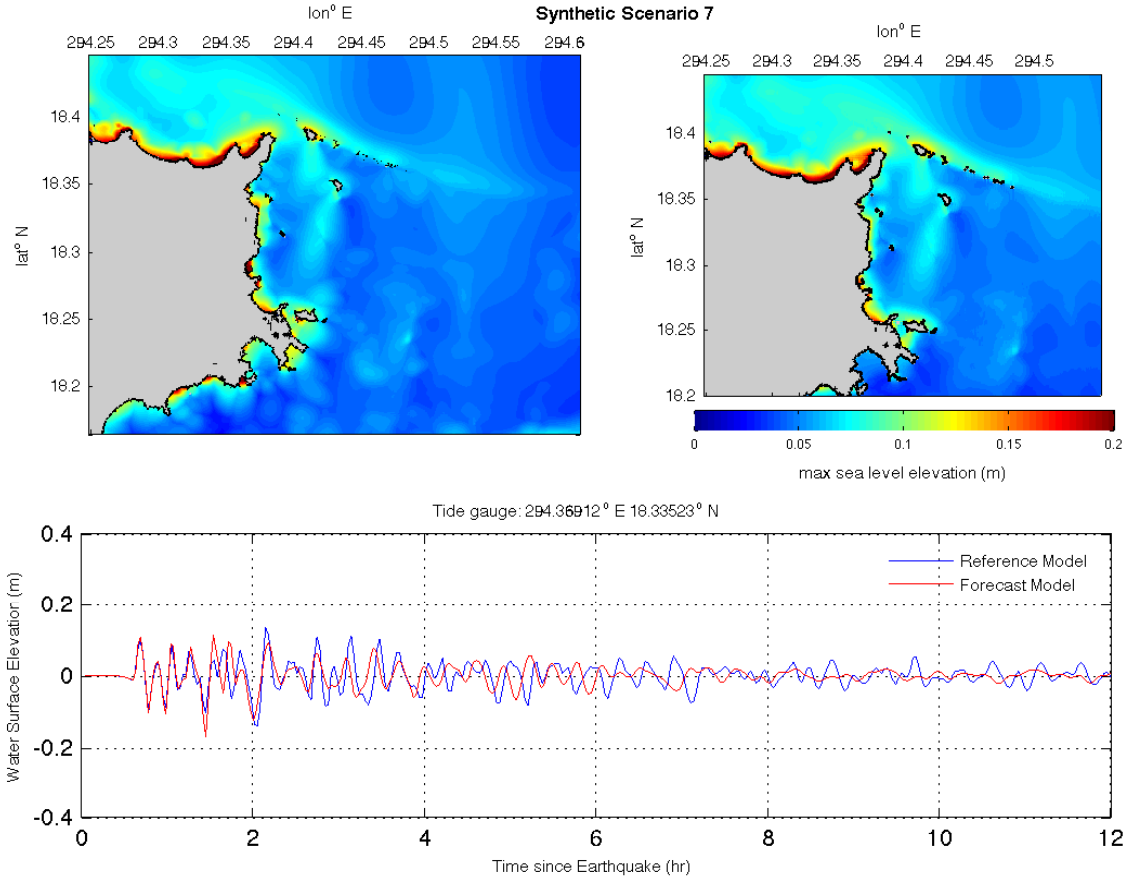

Figure 13: Maximum sea surface elevation computed with the reference (top left) and forecast (top right) models. Comparison at the Fajardo tide gauge of the forecast and reference models for Synthetic Scenario 7 (bottom).

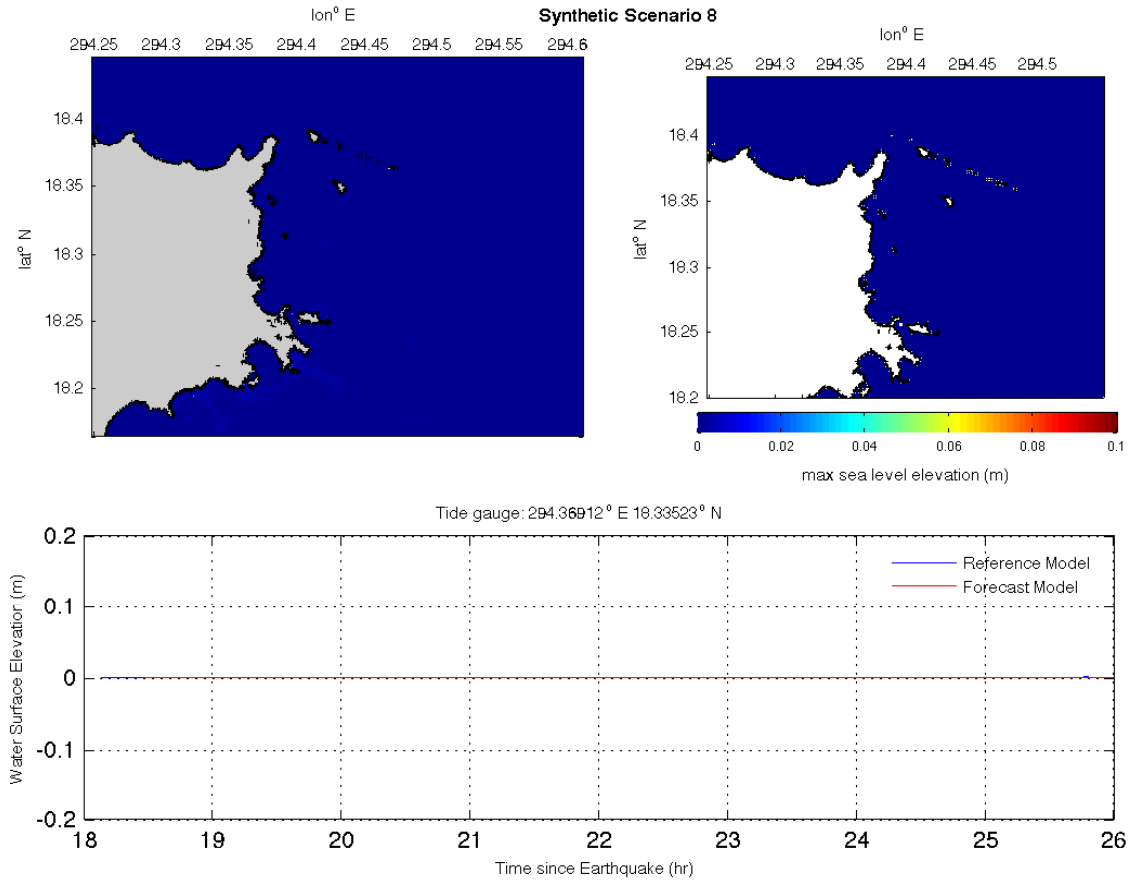

Figure 14: Maximum sea surface elevation computed with the reference (top left) and forecast (top right) models. Comparison at the Fajardo tide gauge of the forecast and reference models for Synthetic Scenario 8 (bottom).

TABLES

Earthquake location	Year	Magnitude
Hispaniola	1953	6.9
Mona Canyon	1946	7.5
Hispaniola	1946	8.1
Mona Canyon	1918	7.5
Anegada Trough	1867	7.5
Puerto Rico Trench	1787	8.1

Table 1: Most significant earthquakes in the Puerto Rico area in the last 3 centuries. Table derived from Mann, 2005

Model Setup	Reference Model			Forecast Model		
	Grid A	**Grid B**	**Grid C**	**Grid A**	**Grid B**	**Grid C**
W	W69.90	W66.92	W66.80	W69.00	W66.87	W66.775
E	W60.50	W66.34	W66.63	W61.00	W66.53	W66.281
S	N18.95	N18.70	N18.52	N18.95	N18.60	N18.522
N	N16.05	N18.28	N18.41	N16.50	N18.35	N18.411
dx	20.97″	6″	1″	47.24″	6″	2″
dy	20″	6″	1″	45″	6″	2″
nx × *ny*	1614×523	351x251	601×401	610×197	201x153	252×201
dt (sec)	2.3	1.23	1.00	5.2	1.58	0.78
D_{min}	1 m			1 m		
Fric. (n^2)	0.0009			0.0009		
CPU Time	~ 114.76 min for 4-hour simulation			~ 11.35 min for 4-hour simulation		
Warning Pt.	W66.70144, N18.47912					

Table 2: MOST setup parameters for reference and forecast models for Fajardo, Puerto Rico.

SceNo.	Scenario Name	Source Zone	Tsunami Source	α (m)	Max (m)	Min (m)
			Mega-tsunami scenario			
1	ATSZ 38-47	Atlantic	A38-A47, B38-B47	25	3.64	-2.38
2	ATSZ 48-57	Atlantic	A48-A57, B48-B57	25	6.24	-2.37
3	ATSZ 58-67	Atlantic	A58-A67, B58-B67	25	2.42	-1.63
4	ATSZ 68-77	Atlantic	A68-A77, B68-B77	25	0.56	-0.46
5	ATSZ 82-91	Atlantic	A82-A91, B82-B91	25	3.12	-2.36
6	SSSZ 1-10	South Sandwich	A1-A10, B1-B10	25	0.74	-0.65
			Mw 7.5 Tsunami scenario			
7	ATSZ B52	Atlantic	B52	1	0.11	-0.17
			Micro-tsunami scenario			
8	SSSZ B11	South Sandwich	B11	0.01	0.0004	-0.0004

Table 3: Synthetic tsunami sources used in the forecast model stability test for Fajardo, Puerto Rico showing tide gauge maximum and minimum water level elevations.

Appendix A

Development of the Fajardo, Puerto Rico tsunami forecast model occurred prior to parameter changes that were made to reflect modifications to the MOST model code. As a result, the input file for running both the tsunami forecast model and the high-resolution reference inundation model in MOST have been updated accordingly. Appendix A1 and A2 provide the updated files for Fajardo.

A.1 Reference model ⋆.in file for Fajardo, Puerto Rico

0.0001 Minimum amplitude of input offshore wave (m)
1 Input minimum depth for offshore (m)
0.1 Input "dry land" depth for inundation (m)
0.0009 Input friction coefficient (n ⋆⋆2)
1 let a and b run up
300.0 max eta before blow up (m)
0.23 Input time step (sec)
190000 Input number of steps
8 Compute "A" arrays every nth time step, n=
1 Compute "B" arrays every nth time step, n=
520 Input number of steps between snapshots
0 ...Starting from
1 ...Saving grid every nth node, n=?
bathy/rim/Anew20s_1nd_SSL1.9sm.asc1.topo
bathy/rim/Grid_B_ref_2s_v3_new.ssl
bathy/rim/Grid_C_ref_1s_v2.dat.ssl.cropped.smth
/home/tg24/data/arcas/store_b2/SRCS/arecibo_srcs/
./rsyn01_run2d/ 1 1 1 1
1
3 439 396

A.2 Forecast model ⋆.in file for Fajardo, Puerto Rico

0.0001 Minimum amplitude of input offshore wave (m)
1 Input minimum depth for offshore (m)

0.1 Input "dry land" depth for inundation (m)
0.0009 Input friction coefficient (n ⋆⋆ 2)
1 let a and b runup
300.0 max eta before blow up (m)
2.1 Input time step (sec)
41150 Input number of steps
2 Compute "A" arrays every nth time step, n=
1 Compute "B" arrays every nth time step, n=
50 Input number of steps between snapshots
1 ...Starting from
1 ...Saving grid every nth node, n=?
bathy_run2d/A5_45s_1nd_SSL1.9.asc.topo1
bathy_run2d//Grid_B_opt_20s_v5.new.ssl
bathy_run2d/Grid_C_opt_3s_v3.dat.ssl
./
./
1 1 1 1 NetCDF output for A, B, C, SIFT
1 Timeseries locations:
3 147 132

Appendix B

Propagation Database: Atlantic Ocean Unit Sources

NOAA Propagation Database presented in this section is the representation of the database as of March, 2013. This database may have been updated since March, 2013.

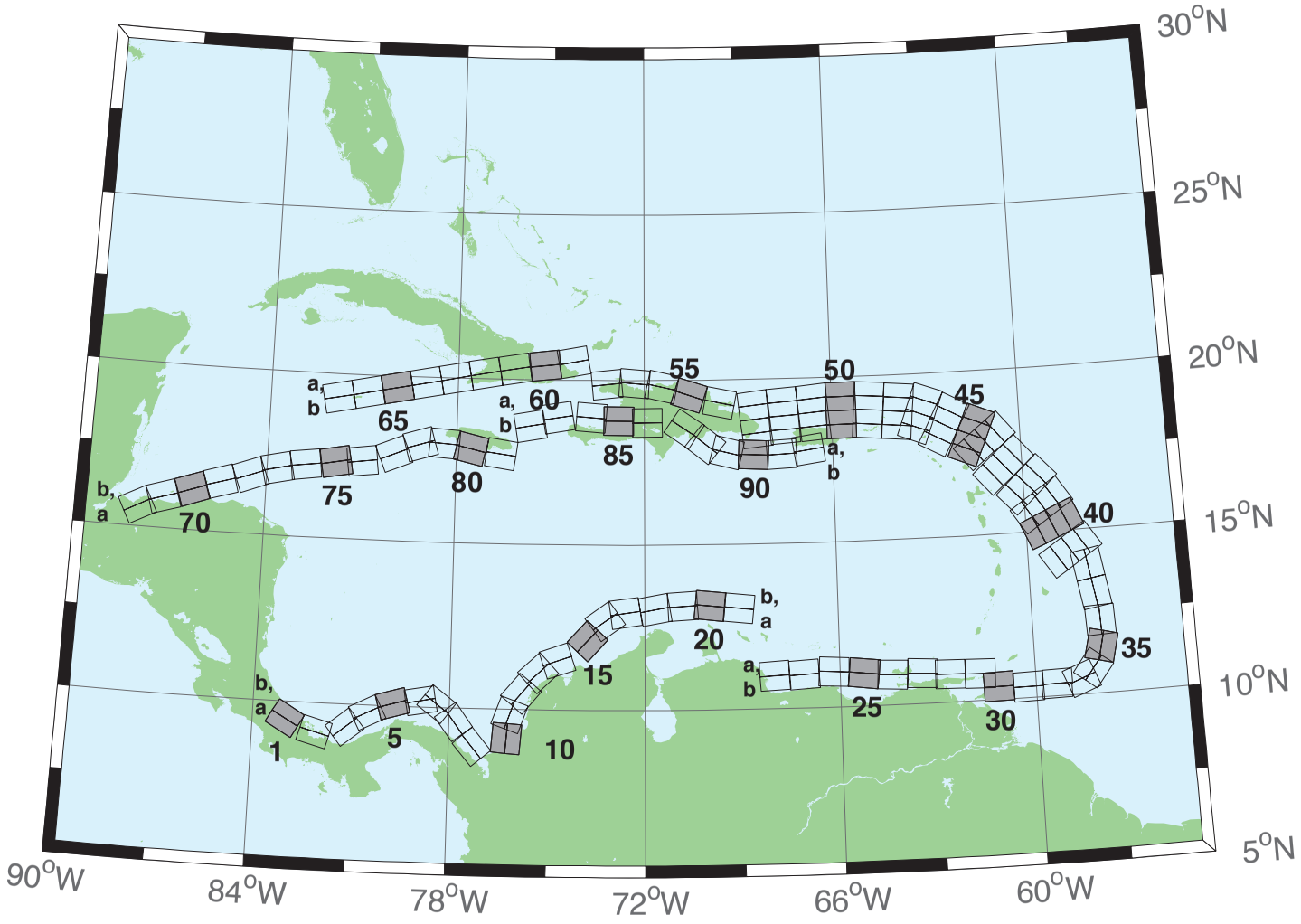

Figure B.1: Atlantic Source Zone unit sources.

Table B.1: Earthquake parameters for Atlantic Source Zone unit sources.

Segment	Description	Longitude(°E)	Latitude(°N)	Strike(°)	Dip(°)	Depth (km)
atsz–1a	Atlantic Source Zone	-83.2020	9.1449	120	27.5	28.09
atsz–1b	Atlantic Source Zone	-83.0000	9.4899	120	27.5	5
atsz–2a	Atlantic Source Zone	-82.1932	8.7408	105.1	27.5	28.09
atsz–2b	Atlantic Source Zone	-82.0880	9.1254	105.1	27.5	5
atsz–3a	Atlantic Source Zone	-80.9172	9.0103	51.31	30	30
atsz–3b	Atlantic Source Zone	-81.1636	9.3139	51.31	30	5
atsz–4a	Atlantic Source Zone	-80.3265	9.4308	63.49	30	30
atsz–4b	Atlantic Source Zone	-80.5027	9.7789	63.49	30	5
atsz–5a	Atlantic Source Zone	-79.6247	9.6961	74.44	30	30
atsz–5b	Atlantic Source Zone	-79.7307	10.0708	74.44	30	5
atsz–6a	Atlantic Source Zone	-78.8069	9.8083	79.71	30	30
atsz–6b	Atlantic Source Zone	-78.8775	10.1910	79.71	30	5
atsz–7a	Atlantic Source Zone	-78.6237	9.7963	127.2	30	30
atsz–7b	Atlantic Source Zone	-78.3845	10.1059	127.2	30	5
atsz–8a	Atlantic Source Zone	-78.1693	9.3544	143.8	30	30
atsz–8b	Atlantic Source Zone	-77.8511	9.5844	143.8	30	5
atsz–9a	Atlantic Source Zone	-77.5913	8.5989	139.9	30	30
atsz–9b	Atlantic Source Zone	-77.2900	8.8493	139.9	30	5
atsz–10a	Atlantic Source Zone	-75.8109	9.0881	4.67	17	19.62
atsz–10b	Atlantic Source Zone	-76.2445	9.1231	4.67	17	5
atsz–11a	Atlantic Source Zone	-75.7406	9.6929	19.67	17	19.62
atsz–11b	Atlantic Source Zone	-76.1511	9.8375	19.67	17	5
atsz–12a	Atlantic Source Zone	-75.4763	10.2042	40.4	17	19.62
atsz–12b	Atlantic Source Zone	-75.8089	10.4826	40.4	17	5
atsz–13a	Atlantic Source Zone	-74.9914	10.7914	47.17	17	19.62
atsz–13b	Atlantic Source Zone	-75.2890	11.1064	47.17	17	5
atsz–14a	Atlantic Source Zone	-74.5666	11.0708	71.68	17	19.62
atsz–14b	Atlantic Source Zone	-74.7043	11.4786	71.68	17	5
atsz–15a	Atlantic Source Zone	-73.4576	11.8012	42.69	17	19.62
atsz–15b	Atlantic Source Zone	-73.7805	12.0924	42.69	17	5
atsz–16a	Atlantic Source Zone	-72.9788	12.3365	54.75	17	19.62
atsz–16b	Atlantic Source Zone	-73.2329	12.6873	54.75	17	5
atsz–17a	Atlantic Source Zone	-72.5454	12.5061	81.96	17	19.62
atsz–17b	Atlantic Source Zone	-72.6071	12.9314	81.96	17	5
atsz–18a	Atlantic Source Zone	-71.6045	12.6174	79.63	17	19.62
atsz–18b	Atlantic Source Zone	-71.6839	13.0399	79.63	17	5
atsz–19a	Atlantic Source Zone	-70.7970	12.7078	86.32	17	19.62
atsz–19b	Atlantic Source Zone	-70.8253	13.1364	86.32	17	5
atsz–20a	Atlantic Source Zone	-70.0246	12.7185	95.94	17	19.62
atsz–20b	Atlantic Source Zone	-69.9789	13.1457	95.94	17	5
atsz–21a	Atlantic Source Zone	-69.1244	12.6320	95.94	17	19.62
atsz–21b	Atlantic Source Zone	-69.0788	13.0592	95.94	17	5
atsz–22a	Atlantic Source Zone	-68.0338	11.4286	266.9	15	17.94
atsz–22b	Atlantic Source Zone	-68.0102	10.9954	266.9	15	5
atsz–23a	Atlantic Source Zone	-67.1246	11.4487	266.9	15	17.94
atsz–23b	Atlantic Source Zone	-67.1010	11.0155	266.9	15	5
atsz–24a	Atlantic Source Zone	-66.1656	11.5055	273.3	15	17.94
atsz–24b	Atlantic Source Zone	-66.1911	11.0724	273.3	15	5
atsz–25a	Atlantic Source Zone	-65.2126	11.4246	276.4	15	17.94
atsz–25b	Atlantic Source Zone	-65.2616	10.9934	276.4	15	5
atsz–26a	Atlantic Source Zone	-64.3641	11.3516	272.9	15	17.94
atsz–26b	Atlantic Source Zone	-64.3862	10.9183	272.9	15	5
atsz–27a	Atlantic Source Zone	-63.4472	11.3516	272.9	15	17.94
atsz–27b	Atlantic Source Zone	-63.4698	10.9183	272.9	15	5
atsz–28a	Atlantic Source Zone	-62.6104	11.2831	271.1	15	17.94
atsz–28b	Atlantic Source Zone	-62.6189	10.8493	271.1	15	5
atsz–29a	Atlantic Source Zone	-61.6826	11.2518	271.6	15	17.94
atsz–29b	Atlantic Source Zone	-61.6947	10.8181	271.6	15	5
atsz–30a	Atlantic Source Zone	-61.1569	10.8303	269	15	17.94
atsz–30b	Atlantic Source Zone	-61.1493	10.3965	269	15	5
atsz–31a	Atlantic Source Zone	-60.2529	10.7739	269	15	17.94

Continued on next page

Table B.1 – continued from previous page

Segment	Description	Longitude(°E)	Latitude(°N)	Strike(°)	Dip(°)	Depth (km)
atsz–31b	Atlantic Source Zone	-60.2453	10.3401	269	15	5
atsz–32a	Atlantic Source Zone	-59.3510	10.8123	269	15	17.94
atsz–32b	Atlantic Source Zone	-59.3734	10.3785	269	15	5
atsz–33a	Atlantic Source Zone	-58.7592	10.8785	248.6	15	17.94
atsz–33b	Atlantic Source Zone	-58.5984	10.4745	248.6	15	5
atsz–34a	Atlantic Source Zone	-58.5699	11.0330	217.2	15	17.94
atsz–34b	Atlantic Source Zone	-58.2179	10.7710	217.2	15	5
atsz–35a	Atlantic Source Zone	-58.3549	11.5300	193.7	15	17.94
atsz–35b	Atlantic Source Zone	-57.9248	11.4274	193.7	15	5
atsz–36a	Atlantic Source Zone	-58.3432	12.1858	177.7	15	17.94
atsz–36b	Atlantic Source Zone	-57.8997	12.2036	177.7	15	5
atsz–37a	Atlantic Source Zone	-58.4490	12.9725	170.7	15	17.94
atsz–37b	Atlantic Source Zone	-58.0095	13.0424	170.7	15	5
atsz–38a	Atlantic Source Zone	-58.6079	13.8503	170.2	15	17.94
atsz–38b	Atlantic Source Zone	-58.1674	13.9240	170.2	15	5
atsz–39a	Atlantic Source Zone	-58.6667	14.3915	146.8	15	17.94
atsz–39b	Atlantic Source Zone	-58.2913	14.6287	146.8	15	5
atsz–39y	Atlantic Source Zone	-59.4168	13.9171	146.8	15	43.82
atsz–39z	Atlantic Source Zone	-59.0415	14.1543	146.8	15	30.88
atsz–40a	Atlantic Source Zone	-59.1899	15.2143	156.2	15	17.94
atsz–40b	Atlantic Source Zone	-58.7781	15.3892	156.2	15	5
atsz–40y	Atlantic Source Zone	-60.0131	14.8646	156.2	15	43.82
atsz–40z	Atlantic Source Zone	-59.6012	15.0395	156.2	15	30.88
atsz–41a	Atlantic Source Zone	-59.4723	15.7987	146.3	15	17.94
atsz–41b	Atlantic Source Zone	-59.0966	16.0392	146.3	15	5
atsz–41y	Atlantic Source Zone	-60.2229	15.3177	146.3	15	43.82
atsz–41z	Atlantic Source Zone	-59.8473	15.5582	146.3	15	30.88
atsz–42a	Atlantic Source Zone	-59.9029	16.4535	137	15	17.94
atsz–42b	Atlantic Source Zone	-59.5716	16.7494	137	15	5
atsz–42y	Atlantic Source Zone	-60.5645	15.8616	137	15	43.82
atsz–42z	Atlantic Source Zone	-60.2334	16.1575	137	15	30.88
atsz–43a	Atlantic Source Zone	-60.5996	17.0903	138.7	15	17.94
atsz–43b	Atlantic Source Zone	-60.2580	17.3766	138.7	15	5
atsz–43y	Atlantic Source Zone	-61.2818	16.5177	138.7	15	43.82
atsz–43z	Atlantic Source Zone	-60.9404	16.8040	138.7	15	30.88
atsz–44a	Atlantic Source Zone	-61.1559	17.8560	141.1	15	17.94
atsz–44b	Atlantic Source Zone	-60.8008	18.1286	141.1	15	5
atsz–44y	Atlantic Source Zone	-61.8651	17.3108	141.1	15	43.82
atsz–44z	Atlantic Source Zone	-61.5102	17.5834	141.1	15	30.88
atsz–45a	Atlantic Source Zone	-61.5491	18.0566	112.8	15	17.94
atsz–45b	Atlantic Source Zone	-61.3716	18.4564	112.8	15	5
atsz–45y	Atlantic Source Zone	-61.9037	17.2569	112.8	15	43.82
atsz–45z	Atlantic Source Zone	-61.7260	17.6567	112.8	15	30.88
atsz–46a	Atlantic Source Zone	-62.4217	18.4149	117.9	15	17.94
atsz–46b	Atlantic Source Zone	-62.2075	18.7985	117.9	15	5
atsz–46y	Atlantic Source Zone	-62.8493	17.6477	117.9	15	43.82
atsz–46z	Atlantic Source Zone	-62.6352	18.0313	117.9	15	30.88
atsz–47a	Atlantic Source Zone	-63.1649	18.7844	110.5	20	22.1
atsz–47b	Atlantic Source Zone	-63.0087	19.1798	110.5	20	5
atsz–47y	Atlantic Source Zone	-63.4770	17.9936	110.5	20	56.3
atsz–47z	Atlantic Source Zone	-63.3205	18.3890	110.5	20	39.2
atsz–48a	Atlantic Source Zone	-63.8800	18.8870	95.37	20	22.1
atsz–48b	Atlantic Source Zone	-63.8382	19.3072	95.37	20	5
atsz–48y	Atlantic Source Zone	-63.9643	18.0465	95.37	20	56.3
atsz–48z	Atlantic Source Zone	-63.9216	18.4667	95.37	20	39.2
atsz–49a	Atlantic Source Zone	-64.8153	18.9650	94.34	20	22.1
atsz–49b	Atlantic Source Zone	-64.7814	19.3859	94.34	20	5
atsz–49y	Atlantic Source Zone	-64.8840	18.1233	94.34	20	56.3
atsz–49z	Atlantic Source Zone	-64.8492	18.5442	94.34	20	39.2
atsz–50a	Atlantic Source Zone	-65.6921	18.9848	89.59	20	22.1
atsz–50b	Atlantic Source Zone	-65.6953	19.4069	89.59	20	5
atsz–50y	Atlantic Source Zone	-65.6874	18.1407	89.59	20	56.3

Continued on next page

Table B.1 – continued from previous page

Segment	Description	Longitude(°E)	Latitude(°N)	Strike(°)	Dip(°)	Depth (km)
atsz–50z	Atlantic Source Zone	-65.6887	18.5628	89.59	20	39.2
atsz–51a	Atlantic Source Zone	-66.5742	18.9484	84.98	20	22.1
atsz–51b	Atlantic Source Zone	-66.6133	19.3688	84.98	20	5
atsz–51y	Atlantic Source Zone	-66.4977	18.1076	84.98	20	56.3
atsz–51z	Atlantic Source Zone	-66.5353	18.5280	84.98	20	39.2
atsz–52a	Atlantic Source Zone	-67.5412	18.8738	85.87	20	22.1
atsz–52b	Atlantic Source Zone	-67.5734	19.2948	85.87	20	5
atsz–52y	Atlantic Source Zone	-67.4781	18.0319	85.87	20	56.3
atsz–52z	Atlantic Source Zone	-67.5090	18.4529	85.87	20	39.2
atsz–53a	Atlantic Source Zone	-68.4547	18.7853	83.64	20	22.1
atsz–53b	Atlantic Source Zone	-68.5042	19.2048	83.64	20	5
atsz–53y	Atlantic Source Zone	-68.3575	17.9463	83.64	20	56.3
atsz–53z	Atlantic Source Zone	-68.4055	18.3658	83.64	20	39.2
atsz–54a	Atlantic Source Zone	-69.6740	18.8841	101.5	20	22.1
atsz–54b	Atlantic Source Zone	-69.5846	19.2976	101.5	20	5
atsz–55a	Atlantic Source Zone	-70.7045	19.1376	108.2	20	22.1
atsz–55b	Atlantic Source Zone	-70.5647	19.5386	108.2	20	5
atsz–56a	Atlantic Source Zone	-71.5368	19.3853	102.6	20	22.1
atsz–56b	Atlantic Source Zone	-71.4386	19.7971	102.6	20	5
atsz–57a	Atlantic Source Zone	-72.3535	19.4838	94.2	20	22.1
atsz–57b	Atlantic Source Zone	-72.3206	19.9047	94.2	20	5
atsz–58a	Atlantic Source Zone	-73.1580	19.4498	84.34	20	22.1
atsz–58b	Atlantic Source Zone	-73.2022	19.8698	84.34	20	5
atsz–59a	Atlantic Source Zone	-74.3567	20.9620	259.7	20	22.1
atsz–59b	Atlantic Source Zone	-74.2764	20.5467	259.7	20	5
atsz–60a	Atlantic Source Zone	-75.2386	20.8622	264.2	15	17.94
atsz–60b	Atlantic Source Zone	-75.1917	20.4306	264.2	15	5
atsz–61a	Atlantic Source Zone	-76.2383	20.7425	260.7	15	17.94
atsz–61b	Atlantic Source Zone	-76.1635	20.3144	260.7	15	5
atsz–62a	Atlantic Source Zone	-77.2021	20.5910	259.9	15	17.94
atsz–62b	Atlantic Source Zone	-77.1214	20.1638	259.9	15	5
atsz–63a	Atlantic Source Zone	-78.1540	20.4189	259	15	17.94
atsz–63b	Atlantic Source Zone	-78.0661	19.9930	259	15	5
atsz–64a	Atlantic Source Zone	-79.0959	20.2498	259.2	15	17.94
atsz–64b	Atlantic Source Zone	-79.0098	19.8236	259.2	15	5
atsz–65a	Atlantic Source Zone	-80.0393	20.0773	258.9	15	17.94
atsz–65b	Atlantic Source Zone	-79.9502	19.6516	258.9	15	5
atsz–66a	Atlantic Source Zone	-80.9675	19.8993	258.6	15	17.94
atsz–66b	Atlantic Source Zone	-80.8766	19.4740	258.6	15	5
atsz–67a	Atlantic Source Zone	-81.9065	19.7214	258.5	15	17.94
atsz–67b	Atlantic Source Zone	-81.8149	19.2962	258.5	15	5
atsz–68a	Atlantic Source Zone	-87.8003	15.2509	62.69	15	17.94
atsz–68b	Atlantic Source Zone	-88.0070	15.6364	62.69	15	5
atsz–69a	Atlantic Source Zone	-87.0824	15.5331	72.73	15	17.94
atsz–69b	Atlantic Source Zone	-87.2163	15.9474	72.73	15	5
atsz–70a	Atlantic Source Zone	-86.1622	15.8274	70.64	15	17.94
atsz–70b	Atlantic Source Zone	-86.3120	16.2367	70.64	15	5
atsz–71a	Atlantic Source Zone	-85.3117	16.1052	73.7	15	17.94
atsz–71b	Atlantic Source Zone	-85.4387	16.5216	73.7	15	5
atsz–72a	Atlantic Source Zone	-84.3470	16.3820	69.66	15	17.94
atsz–72b	Atlantic Source Zone	-84.5045	16.7888	69.66	15	5
atsz–73a	Atlantic Source Zone	-83.5657	16.6196	77.36	15	17.94
atsz–73b	Atlantic Source Zone	-83.6650	17.0429	77.36	15	5
atsz–74a	Atlantic Source Zone	-82.7104	16.7695	82.35	15	17.94
atsz–74b	Atlantic Source Zone	-82.7709	17.1995	82.35	15	5
atsz–75a	Atlantic Source Zone	-81.7297	16.9003	79.86	15	17.94
atsz–75b	Atlantic Source Zone	-81.8097	17.3274	79.86	15	5
atsz–76a	Atlantic Source Zone	-80.9196	16.9495	82.95	15	17.94
atsz–76b	Atlantic Source Zone	-80.9754	17.3801	82.95	15	5
atsz–77a	Atlantic Source Zone	-79.8086	17.2357	67.95	15	17.94
atsz–77b	Atlantic Source Zone	-79.9795	17.6378	67.95	15	5
atsz–78a	Atlantic Source Zone	-79.0245	17.5415	73.61	15	17.94

Continued on next page

Table B.1 – continued from previous page

Segment	Description	Longitude(°E)	Latitude(°N)	Strike(°)	Dip(°)	Depth (km)
atsz–78b	Atlantic Source Zone	-79.1532	17.9577	73.61	15	5
atsz–79a	Atlantic Source Zone	-78.4122	17.5689	94.07	15	17.94
atsz–79b	Atlantic Source Zone	-78.3798	18.0017	94.07	15	5
atsz–80a	Atlantic Source Zone	-77.6403	17.4391	103.3	15	17.94
atsz–80b	Atlantic Source Zone	-77.5352	17.8613	103.3	15	5
atsz–81a	Atlantic Source Zone	-76.6376	17.2984	98.21	15	17.94
atsz–81b	Atlantic Source Zone	-76.5726	17.7278	98.21	15	5
atsz–82a	Atlantic Source Zone	-75.7299	19.0217	260.1	15	17.94
atsz–82b	Atlantic Source Zone	-75.6516	18.5942	260.1	15	5
atsz–83a	Atlantic Source Zone	-74.8351	19.2911	260.8	15	17.94
atsz–83b	Atlantic Source Zone	-74.7621	18.8628	260.8	15	5
atsz–84a	Atlantic Source Zone	-73.6639	19.2991	274.8	15	17.94
atsz–84b	Atlantic Source Zone	-73.7026	18.8668	274.8	15	5
atsz–85a	Atlantic Source Zone	-72.8198	19.2019	270.6	15	17.94
atsz–85b	Atlantic Source Zone	-72.8246	18.7681	270.6	15	5
atsz–86a	Atlantic Source Zone	-71.9143	19.1477	269.1	15	17.94
atsz–86b	Atlantic Source Zone	-71.9068	18.7139	269.1	15	5
atsz–87a	Atlantic Source Zone	-70.4738	18.8821	304.5	15	17.94
atsz–87b	Atlantic Source Zone	-70.7329	18.5245	304.5	15	5
atsz–88a	Atlantic Source Zone	-69.7710	18.3902	308.9	15	17.94
atsz–88b	Atlantic Source Zone	-70.0547	18.0504	308.4	15	5
atsz–89a	Atlantic Source Zone	-69.2635	18.2099	283.9	15	17.94
atsz–89b	Atlantic Source Zone	-69.3728	17.7887	283.9	15	5
atsz–90a	Atlantic Source Zone	-68.5059	18.1443	272.9	15	17.94
atsz–90b	Atlantic Source Zone	-68.5284	17.7110	272.9	15	5
atsz–91a	Atlantic Source Zone	-67.6428	18.1438	267.8	15	17.94
atsz–91b	Atlantic Source Zone	-67.6256	17.7103	267.8	15	5
atsz–92a	Atlantic Source Zone	-66.8261	18.2536	262	15	17.94
atsz–92b	Atlantic Source Zone	-66.7627	17.8240	262	15	5

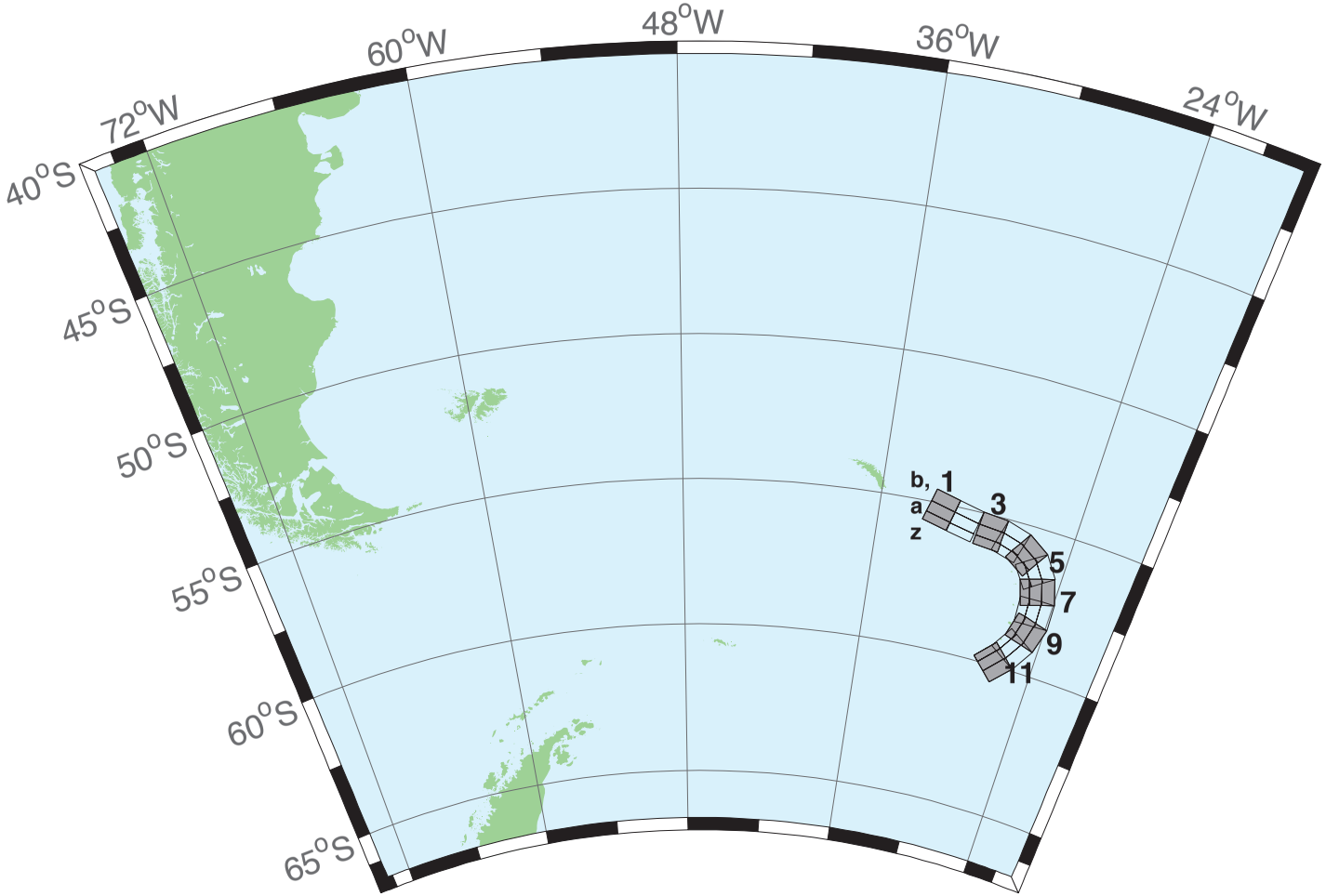

Figure B.2: South Sandwich Islands Subduction Zone.

Table B.2: Earthquake parameters for South Sandwich Islands Subduction Zone unit sources.

Segment	Description	Longitude(°E)	Latitude(°N)	Strike(°)	Dip(°)	Depth (km)
sssz–1a	South Sandwich Islands Subduction Zone	-32.3713	-55.4655	104.7	28.53	17.51
sssz–1b	South Sandwich Islands Subduction Zone	-32.1953	-55.0832	104.7	9.957	8.866
sssz–1z	South Sandwich Islands Subduction Zone	-32.5091	-55.7624	104.7	46.99	41.39
sssz–2a	South Sandwich Islands Subduction Zone	-30.8028	-55.6842	102.4	28.53	17.51
sssz–2b	South Sandwich Islands Subduction Zone	-30.6524	-55.2982	102.4	9.957	8.866
sssz–2z	South Sandwich Islands Subduction Zone	-30.9206	-55.9839	102.4	46.99	41.39
sssz–3a	South Sandwich Islands Subduction Zone	-29.0824	-55.8403	95.53	28.53	17.51
sssz–3b	South Sandwich Islands Subduction Zone	-29.0149	-55.4468	95.53	9.957	8.866
sssz–3z	South Sandwich Islands Subduction Zone	-29.1353	-56.1458	95.53	46.99	41.39
sssz–4a	South Sandwich Islands Subduction Zone	-27.8128	-55.9796	106.1	28.53	17.51
sssz–4b	South Sandwich Islands Subduction Zone	-27.6174	-55.5999	106.1	9.957	8.866
sssz–4z	South Sandwich Islands Subduction Zone	-27.9659	-56.2744	106.1	46.99	41.39
sssz–5a	South Sandwich Islands Subduction Zone	-26.7928	-56.2481	123.1	28.53	17.51
sssz–5b	South Sandwich Islands Subduction Zone	-26.4059	-55.9170	123.1	9.957	8.866
sssz–5z	South Sandwich Islands Subduction Zone	-27.0955	-56.5052	123.1	46.99	41.39
sssz–6a	South Sandwich Islands Subduction Zone	-26.1317	-56.6466	145.6	23.28	16.11
sssz–6b	South Sandwich Islands Subduction Zone	-25.5131	-56.4133	145.6	9.09	8.228
sssz–6z	South Sandwich Islands Subduction Zone	-26.5920	-56.8194	145.6	47.15	35.87
sssz–7a	South Sandwich Islands Subduction Zone	-25.6787	-57.2162	162.9	21.21	14.23
sssz–7b	South Sandwich Islands Subduction Zone	-24.9394	-57.0932	162.9	7.596	7.626
sssz–7z	South Sandwich Islands Subduction Zone	-26.2493	-57.3109	162.9	44.16	32.32
sssz–8a	South Sandwich Islands Subduction Zone	-25.5161	-57.8712	178.2	20.33	15.91
sssz–8b	South Sandwich Islands Subduction Zone	-24.7233	-57.8580	178.2	8.449	8.562
sssz–8z	South Sandwich Islands Subduction Zone	-26.1280	-57.8813	178.2	43.65	33.28
sssz–9a	South Sandwich Islands Subduction Zone	-25.6657	-58.5053	195.4	25.76	15.71
sssz–9b	South Sandwich Islands Subduction Zone	-24.9168	-58.6127	195.4	8.254	8.537
sssz–9z	South Sandwich Islands Subduction Zone	-26.1799	-58.4313	195.4	51.69	37.44
sssz–10a	South Sandwich Islands Subduction Zone	-26.1563	-59.1048	212.5	32.82	15.65
sssz–10b	South Sandwich Islands Subduction Zone	-25.5335	-59.3080	212.5	10.45	6.581
sssz–10z	South Sandwich Islands Subduction Zone	-26.5817	-58.9653	212.5	54.77	42.75
sssz–11a	South Sandwich Islands Subduction Zone	-27.0794	-59.6799	224.2	33.67	15.75
sssz–11b	South Sandwich Islands Subduction Zone	-26.5460	-59.9412	224.2	11.32	5.927
sssz–11z	South Sandwich Islands Subduction Zone	-27.4245	-59.5098	224.2	57.19	43.46

Appendix C

SIFT Testing

Lindsey Wright

C.1 Purpose

Forecast models are tested with synthetic tsunami events covering a range of tsunami source locations. Testing is also done with selected historical tsunami events when available.

The purpose of forecast model testing is three-fold. The first objective is to assure that the results obtained with NOAA tsunami forecast system, which has been released to the Tsunami Warning Centers for operational use, are identical to those obtained by the researcher during the development of the forecast model. The second objective is to test the forecast model for consistency, accuracy, time efficiency, and quality of results over a range of possible tsunami locations and magnitudes. The third objective is to identify bugs and issues in need of resolution by the researcher who developed the forecast model or by the forecast software development team before the next version release to NOAA's two Tsunami Warning Centers.

Local hardware and software applications, and tools familiar to the researcher(s), are used to run the Method of Splitting Tsunami (MOST) model during the forecast model development. The test results presented in this report lend confidence that the model performs as developed and produces the same results when initiated within the forecast application in an operational setting as those produced by the researcher during the forecast model development. The test results assure those who rely on the Fajardo, Puerto Rico tsunami forecast model that consistent results are produced irrespective of system.

C.2 Testing Procedure

The general procedure for forecast model testing is to run a set of synthetic tsunami scenarios through the forecast system application and compare the results with those obtained by the researcher during the forecast model development and presented in the Tsunami Forecast Model Report. Specific steps taken to test the model include:

1. Identification of testing scenarios, including the standard set of synthetic events and customized synthetic scenarios that may have been used by the researcher(s) in developing the forecast model.

2. Creation of new events to represent customized synthetic scenarios used by the researcher(s) in developing the forecast model, if any.

3. Submission of test model runs with the forecast system, and export of the results from A, B, and C grids, along with time series.

4. Recording applicable metadata, including the specific version of the forecast system used for testing.

5. Examination of forecast model results from the forecast system for instabilities in both time series and plot results.

6. Comparison of forecast model results obtained through the forecast system with those obtained during the forecast model development.

7. Summarization of results with specific mention of quality, consistency, and time efficiency.

8. Reporting of issues identified to modeler and forecast software development team.

9. Retesting the forecast models in the forecast system when reported issues have been addressed or explained.

Synthetic model runs were tested on a DELL PowerEdge R510 computer equipped with two Xeon E5670 processors at 2.93 Ghz, each with 12 MBytes of cache and 32 GB memory. The processors are hex core and support hyperthreading, resulting in the computer performing as a 24 processor core machine. Additionally, the testing computer supports 10 Gigabit Ethernet for fast network connections. This computer configuration is similar or the same as the configurations of the computers installed at the Tsunami Warning Centers so the compute times should only vary slightly

C.3 Results

The Fajardo forecast model was tested with SIFT version 3.2.

A suite of three synthetic events was run on the Fajardo forecast model. Test results from the forecast system and comparisons with the results obtained during the forecast model development are shown numerically in Table C.1 and graphically in Figures C.1 to C.3. The results show that the minimum and maximum amplitudes and time series obtained from the forecast system agree with those obtained during the forecast model development, and that the forecast model is stable and robust, with consistent and high quality results across geographically distributed tsunami sources. The model run time (wall-clock time) was 25 min for 12 hr of simulation time, and 8.3 minutes for 4.0 hr. This run time is within the 10 minute run time for 4 hours of simulation time and satisfies run time requirements.

The modeled scenarios were stable for all cases run with no inconsistencies or ringing. Two of the three scenarios tested produced wave heights greater than 350 (cm). The largest modeled height was 624 cm from the Atlantic (ATSZ 48-57) source zone and the smallest signal of 76 cm originated from the far-field South Sandwich (SSSZ 1-10) source zone. Comparisons between the development cases and the forecast system output were consistent in shape and amplitude

for all cases run. The Fajardo reference point used for the forecast model development is the same as what is currently deployed in the forecast system, so the results can be considered valid for the three cases studied.

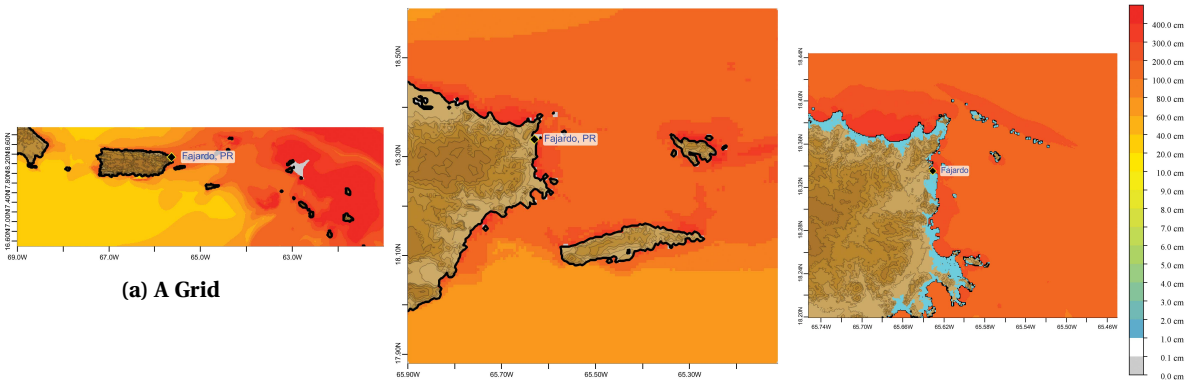

(a) A Grid

(b) B Grid

(c) C Grid

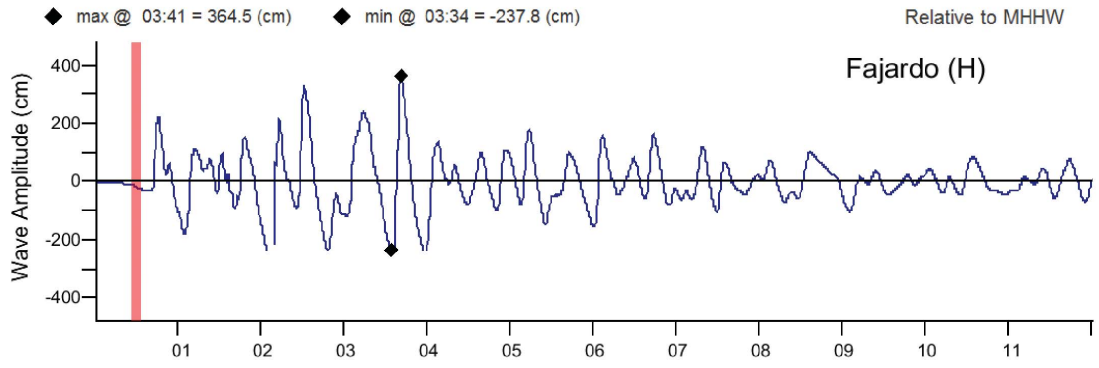

(d)

Figure C.1: Response of the Fajardo, Puerto Rico forecast model to synthetic scenario ATSZ 38-47 (alpha=25). Maximum sea surface elevation for (a) A-grid, b) B-grid, c) C-grid. Sea surface elevation time series at the C-grid warning point (d). The lower time series plot is the result obtained during model development and is shown for comparison with test results.

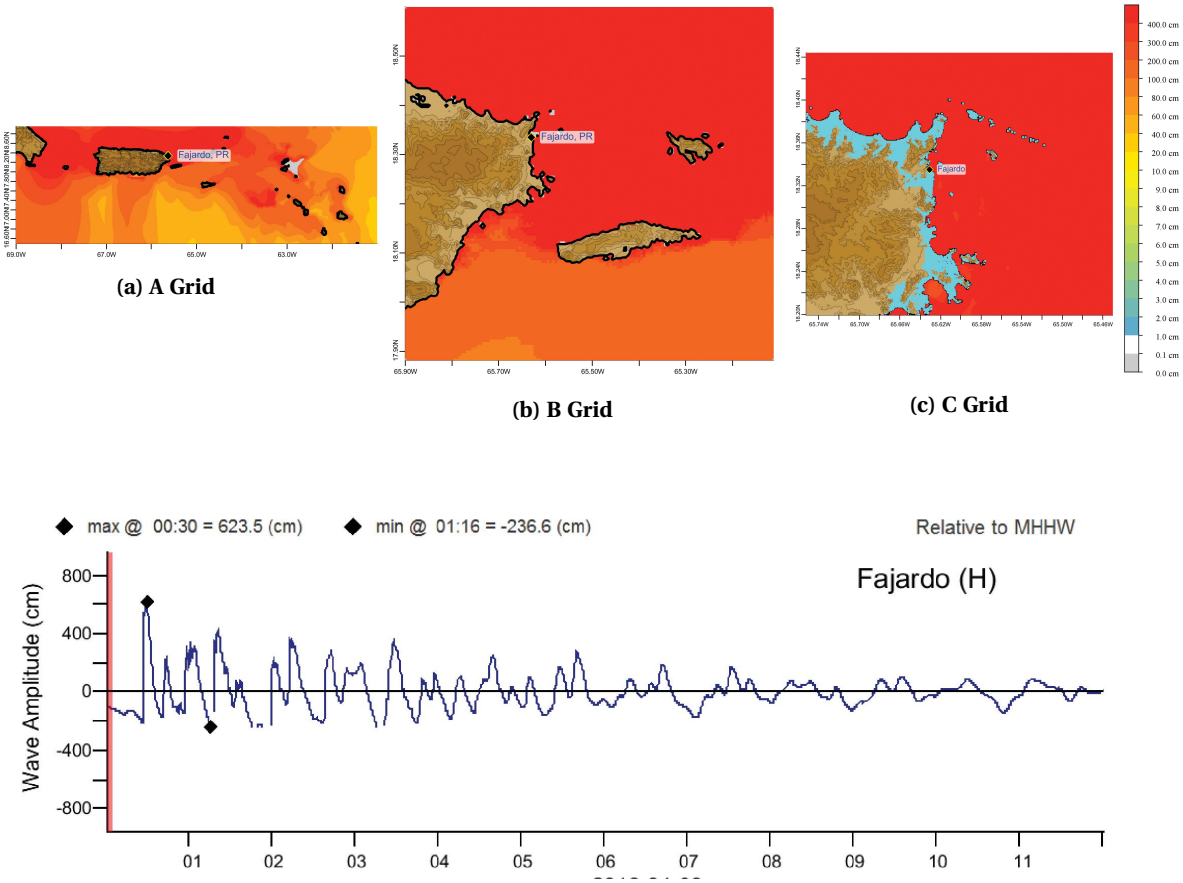

(a) A Grid

(b) B Grid

(c) C Grid

(d)

Figure C.2: Response of the Fajardo, Puerto Rico forecast model to synthetic scenario ATSZ 48-57 (alpha=25). Maximum sea surface elevation for (a) A-grid, b) B-grid, c) C-grid. Sea surface elevation time series at the C-grid warning point (d). The lower time series plot is the result obtained during model development and is shown for comparison with test

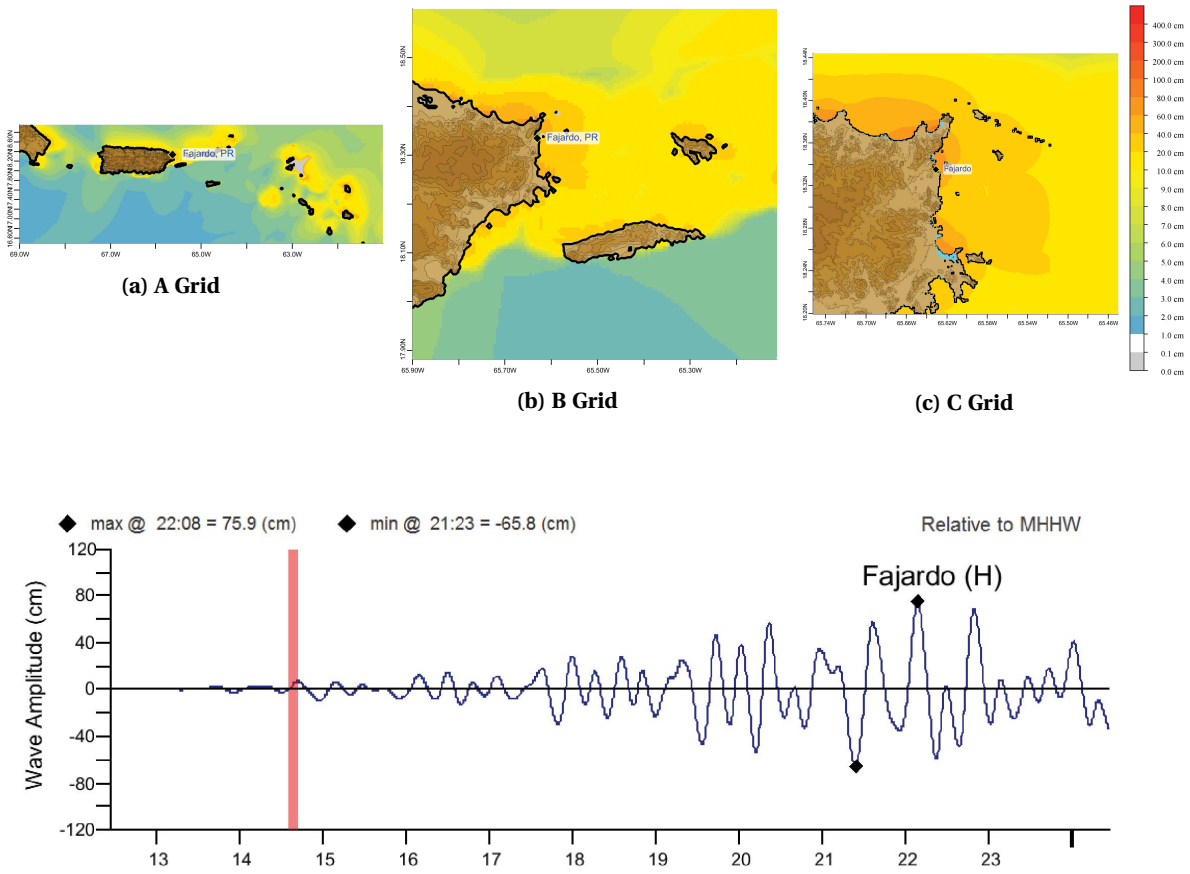

(a) A Grid **(b) B Grid** **(c) C Grid**

Figure C.3: Response of the Fajardo, Puerto Rico forecast model to synthetic scenario SSSZ 1-10 (alpha=25). Maximum sea surface elevation for (a) A-grid, b) B-grid, c) C-grid. Sea surface elevation time series at the C-grid warning point (d). The lower time series plot is the result obtained during model development and is shown for comparison with test results.

Scenario Name	Source Zone	Tsunami Source	α [m]	SIFT Max (cm)	Development Max (cm)	SIFT Min (cm)	Development Min (cm)
Mega-tsunami Scenarios							
ATSZ 38-47	Atlantic	A38-A47, B38-B47	25	364.5		-237.8	
ATSZ 48-57	Atlantic	A48-A57, B48-B57	25	623.5		-236.6	
SSSZ 1-10	South Sandwich	A1-A10, B1-B10	25	75.9		-65.8	

Table C.1: Table of maximum and minimum amplitudes (cm) at the Fajardo, Puerto Rico warning point for synthetic and historical events tested using SIFT 3.2 and obtained during development.

Appendix D

Energy Propagation Pattern

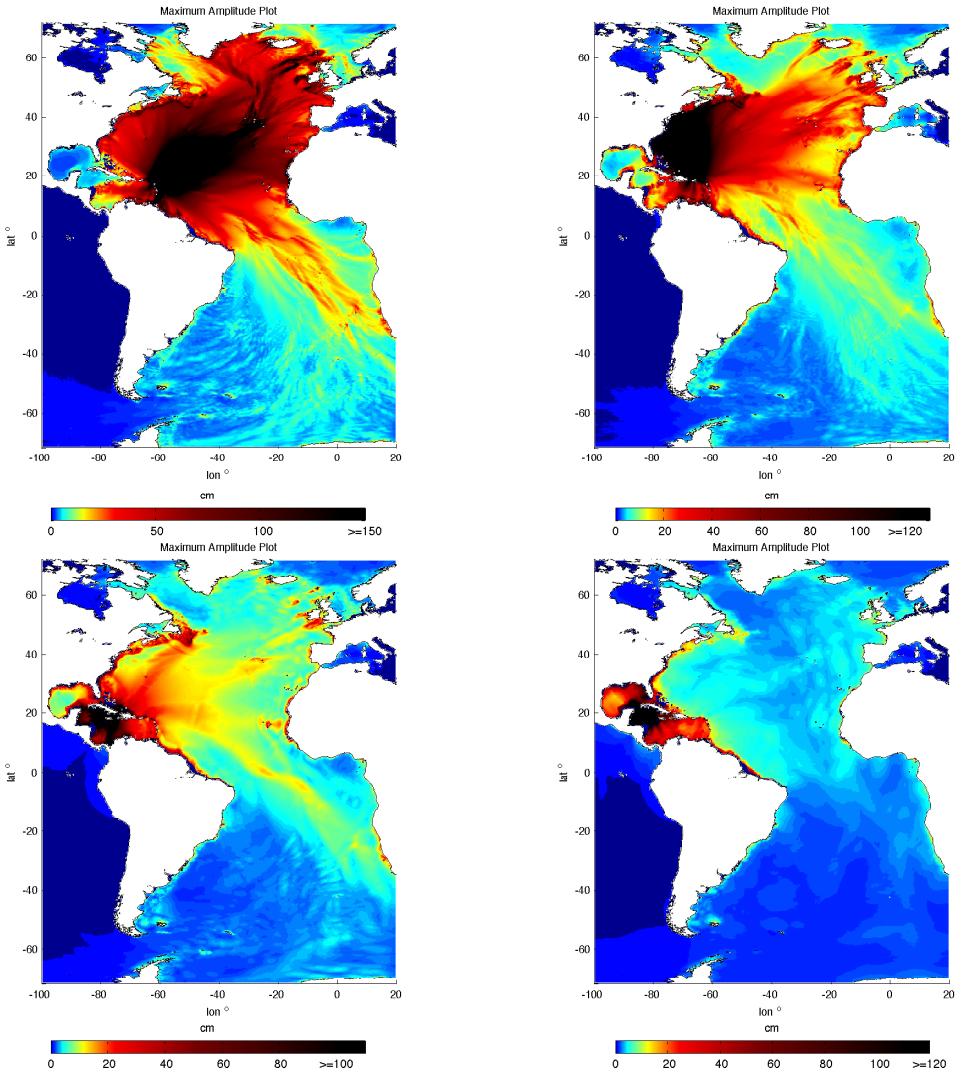

Figure D.1: Energy propagation patterns throughout the Pacific Ocean for four synthetic mega-tsunami scenarios used during the Fajardo, PR forecast model development. Upper left panel is Case 1 of Table 3 (ATSZ 38-47), upper right panel is Case 2 (ATSZ 48-57), lower left is Case 3 (ATSZ 58-67) and lower right is Case 4 (ATSZ 68-77). Synthetic scenario 2 represents the worst case for Fajardo, situated on the northern coast of Puerto Rico.

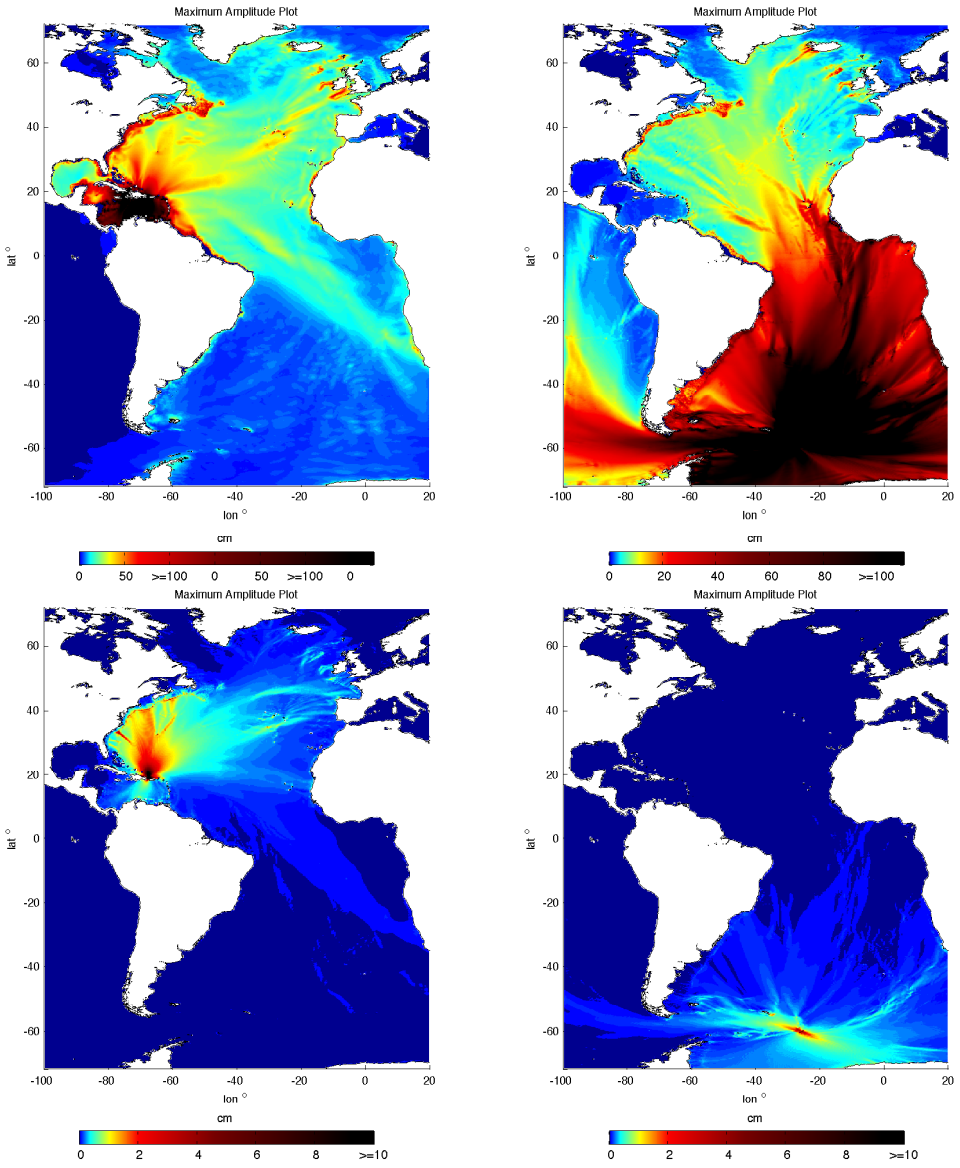

Figure D.2: Energy propagation patterns throughout the Pacific Ocean for two synthetic mega-tsunami scenarios (upper panels), one Mw 7.5 scenario (lower left panel), and one micro-tsunami scenario (lower right panel) used during the Fajardo, PR forecast model development. Upper left panel is Case 5 of Table 3 (ATSZ 82-91), upper right panel is Case 6 (SSSZ 1-10), lower left is Case 7 (ATSZ B52) and lower right is Case 8 (SSSZ B11).